J|A|C|S
ARTICLES
Published on Web 03/26/2004

α-Turn Mimetics: Short Peptide α-Helices Composed of Cyclic Metallopentapeptide Modules

Michael J. Kelso,[†] Renée L. Beyer,[†] Huy N. Hoang,[†,‡] Ami S. Lakdawala,[§] James P. Snyder,[§] Warren V. Oliver,[†] Tom A. Robertson,[†] Trevor G. Appleton,[‡] and David P. Fairlie*[,†]

Contribution from the Centre for Drug Design and Development, Institute for Molecular Bioscience and Department of Chemistry, University of Queensland, Brisbane, Qld 4072, Australia, and Department of Chemistry, Emory University, Atlanta, Georgia 30322

Received August 18, 2003; E-mail: d.fairlie@imb.uq.edu.au

Abstract: α-Helices are key structural components of proteins and important recognition motifs in biology. Short peptides (≤15 residues) corresponding to these helical sequences are rarely helical away from their stabilizing protein environments. New techniques for stabilizing short peptide helices could be valuable for studying protein folding, modeling proteins, creating artificial proteins, and may aid the design of inhibitors or mimics of protein function. This study reports the facile incorporation of 3- and 4-α turns in 10−15 residue peptides through formation in situ of multiple cyclic metallopeptide modules $[Pd(en)(H*XXXH*)]^{2+}$. The nonhelical peptides Ac-H*ELTH*H*VTDH*-NH_2 (**1**), Ac-H*ELTH*AVTDYH*ELTH*-NH_2 (**2**), and Ac-H*AAAH*H*ELTH*H*VTDH*-NH_2 (**3**) (H* is histidine-methylated at imidazole-N3) react in *N*,*N*-dimethylformamide (DMF) or water with 2, 2, and 3 molar equivalents, respectively, of $[Pd(en)(NO_3)_2]$ to form exclusively $[Pd_2(en)_2$(Ac-H*ELTH*H*VTDH*-$NH_2)]^{4+}$ (**4**), $[Pd_2(en)_2$(Ac-H*ELTH*AVTDYH*ELTH*-$NH_2)]^{4+}$ (**5**), and $[Pd_3(en)_3$(Ac-H*AAAH*H*ELTH*H*VTDH*-$NH_2)]^{6+}$ (**6**), characterized by mass spectrometry, 1D and 2D ^{1}H- and 1D ^{15}N-NMR spectroscopy. Despite the presence of multiple histidines and other possible metal-binding residues in these peptides, 2D ^{1}H NMR spectra reveal that $Pd(en)^{2+}$ is remarkably specific in coordinating to imidazole-N1 of only (*i*, *i* + 4) pairs of histidines (i.e., only those separated by three amino acids), resulting in **4**−**6** made up of cyclic metallopentapeptide modules $([Pd(en)(H*XXXH*)]^{2+})_n$, $n = 2$, 2, 3, respectively, each cycle being a 22-membered ring. We have previously shown that a single metallopentapeptide can nucleate α-helicity (Kelso et al., *Angew. Chem., Int. Ed.* **2003**, *42*, 421−424.). We now demonstrate its use as an α-turn-mimicking module for the facile conversion of unstructured short peptides into helices of macrocycles and provide 1D and 2D NMR spectroscopic data, structure calculations via XPLOR and NMR analysis of molecular flexibility in solution (NAMFIS), and CD spectra in support of the α-helical nature of these monomeric metallopeptides in solution.

Introduction

The α-helix is a fundamental structural unit in the fabric of proteins, with 30% of all amino acids in proteins occurring in α-helices.[1] When buried in the hydrophobic interiors of proteins, helices play crucial structure-stabilizing roles, act as templates for folding proteins, and help to create active sites of enzymes. When partially exposed on the surfaces of proteins, helices are often key functional motifs that are recognized by other proteins, RNA, or DNA, interactions that can mediate important biological processes.[2] For example, transcriptional activators (e.g., p53, NF-kBp65, VP16c)[3] apoptosis regulators (e.g., Bak),[4] and RNA-transporter proteins (e.g., Rev)[5] all contain a short α-helical sequence that mediates function by direct interaction with a receptor.

Short peptides (<15 amino acids) corresponding to these helical protein regions are difficult to study because they tend to adopt only random structures in solution when removed from their protein environments.[6] Attempts to produce short α-helices by using helix-capping templates,[7] unnatural amino acids,[8] noncovalent side-chain constraints (e.g., salt bridges, hydro-

[†] Centre for Drug Design and Development, Institute for Molecular Bioscience, University of Queensland.
[‡] Department of Chemistry, University of Queensland.
[§] Emory University.

(1) Barlow, D. J.; Thornton, J. M. *J. Mol. Biol.* **1988**, *201*, 601.
(2) (a) Fairlie, D.; West, M.; Wong, A. *Curr. Med. Chem.* **1998**, *5*, 29. (b) Andrews, M. J. I.; Tabor, A. B. *Tetrahedron* **1999**, *55*, 11711.
(3) (a) Kussie, P. H.; Gorina, S.; Marechal, V.; Elenbaas, B.; Moreau, J.; Levine, A. J.; Pavletich, N. P. *Science* **1996**, *274*, 948. (b) Burley, S. K.; Roeder, R. G. *Annu. Rev. Biochem.* **1996**, *65*, 769. (c) Uesugi, M.; Nyaguile, O.; Lu, H.; Levine, A. J.; Verdine, G. L. *Science* **1997**, *277*, 1310.
(4) Sattler, M.; Liang, H.; Nettesheim, D.; Meadows, R. P.; Harlan, J. E.; Eberstadt, M.; Yoon, H. S.; Shuker, S. B.; Chang, B. S.; Minn, A. J.; Thompson, C. B.; Fesik, S. W. *Science* **1997**, *275*, 983.
(5) Tan, R.; Chen, L.; Buettner, J. A.; Hudson, D.; Frankel, A. D. *Cell* **1993**, *73*, 1031.
(6) (a) Zimm, B.; Bragg, J. *J. Chem. Phys.* **1959**, *31*, 526. (b) Scholtz, A.; Baldwin, R. L. *Annu. Rev. Biophys. Biomol. Struct.* **1992**, *21*, 95.
(7) (a) Kemp, D.; Curran, T.; Boyd, J.; Allen, T. *J. Org. Chem.* **1991**, *56*, 6683. (b) Müller, K.; Obrecht, D.; Knierzinger, A.; Stankovic, C.; Spiegler, C.; Bannwarth, W.; Trzeciak, A.; Englert, G.; Labhardt, A. M.; Schoenholzer, P. *Perspect. Med. Chem.* **1993**, 513. (c) Austin, R.; Maplestone, R. A.; Sefler, A. M.; Liu, K.; Hruzewicz, W. N.; Liu, C.; Cho, H. S.; Wemmer, D. E.; Bartlett, P. A. *J. Am. Chem. Soc.* **1997**, *119*, 6461. (d) Aurora, R.; Rose, G. D. *Protein Sci.* **1998**, *7*, 21.

10.1021/ja037980i CCC: $27.50 **© 2004 American Chemical Society**

phobic interactions),[9] covalent side-chain linkers (e.g., disulfide,[10] hydrazone,[11] lactam bridges[12]), or nonpeptidic replacements for the helical scaffold[13] have met with some success for specific peptides, but generic strategies for helix stabilization remain elusive.

Another approach to stabilizing peptide helices is to use metal ions to "clip" together metal-ligating side chains that reside on the same face of a helix (e.g., i, $i + 4$ positions). This approach has received relatively little attention despite nature often using metal ions (e.g., Zn^{2+}) to bind to the imidazole N1-nitrogens of two (i, $i + 4$) spaced histidines in protein α-helices.[14] The reported preference for metals in forming only small (five- and six-membered) chelate rings when binding to histidines in peptides, rather than the larger macrocycles found in proteins, may explain the paucity of studies in this field, the consensus being that metal ions interact differently with proteins than with short peptides.[15]

There are only a few reports where metal ions are purported to stabilize native or synthetically modified short, usually Ala-rich, peptides in an α-helical conformation. In those cases the metals were presumed, though not proven, to form macrocyclic chelates by coordinating to two amino acid side chains separated by three intervening residues in a sequence (e.g., at i and $i + 4$ positions as in HxxxH).[16] We previously communicated[17a] that a test pentapeptide Ac-HAAAH-NH_2 reacts with [Pd(en)$(NO_3)_2$] in *N*,*N*-dimethylformamide (DMF)-d_7 to produce three linkage isomeric complexes of [Pd(en)(Ac-HAAAH-NH_2)]$^{2+}$, in which two His residues are coordinated to Pd(II) via imidazole nitrogens N1 and N1, N1 and N3, or N3 and N1, creating the unusual 22-, 21-, and 21-membered macrocycles. 2D NMR spectroscopy coupled to simulated annealing for the most prevalent metallopentapeptide isomer (N1-imidazole of both histidines coordinated to Pd^{2+}) suggested a helical structure in DMF. An alternative conformational analysis did not confirm the presence of α-helix.[18] We extended the work[17b] to different 5−15 residue peptides corresponding to the Zn-binding domain of thermolysin and demonstrated that Pd(II) coordinates N1-imidazole nitrogens to form a 22-membered [Pd(en)-(H*ELTH*)]$^{2+}$ macrocycle that simulated annealing suggested to be helical in solution.[19] This macrocycle acts as a template in nucleating α-helicity in both C- and N-terminal directions within longer sequences in DMF.[17b] In water, however, there was much less α-helicity observed, testifying to the difficulty of fixing intramolecular amide NH···OC H-bonds in a solvent-exposed sequence in competition with the excellent H-bond donor water.

To expand the utility of [Pd(en)(H*xxxH*)]$^{2+}$ as a helix-promoting module in solution, we were particularly interested in discovering: (a) whether such modules could be regioselectively created in situ within peptides consisting of multiple potential metal-binding residues, including 4−6 His residues and (b) whether multiple units of the helical module [Pd(en)-(H*xxxH*)]$^{2+}$ would further increase α-helicity even in water. For comparison with previous work,[17] we chose to study peptides incorporating the same pentapeptide sequences reported on before including the test sequence[17a] H*AAAH*, the zinc-binding domain H*ELTH* of thermolysin,[17b] and one other sequence H*VTDH* with sufficiently different residues to enable signal dispersion in NOESY spectra. The sequence H*ELTH*AVTDY is a fragment of thermolysin that we have reported on before.[17b] A feature of these sequences was the replacement of histidine (H) with histidine methylated at imidazole N3 (H*) to avoid complications from linkage isomers noted above and encourage coordination through N1 of imidazole.

We now report on three sequences involving multiple potential metal-binding domains composed of residues from the zinc-binding region of thermolysin, namely Ac-H*ELTH*H*-VTDH*-NH_2 (**1**), Ac-H*ELTH*AVTDYH*ELTH*-NH_2 (**2**), and Ac-H*AAAH*H*ELTH*H*VTDH*-NH_2 (**3**). Each of these react with multiple equivalents of [Pd(en)$(ONO_2)_2$] to produce exclusively **4**−**6**, respectively (Chart 1), in both DMF-d_7 and water (90% H_2O, 10% D_2O). Mass spectrometry, 1D ^{15}N- and 2D ^{1}H-NMR spectroscopy, and circular dichroism (CD) spectra were used to characterize the structures **4**−**6**, and their three-dimensional structures were calculated from NOE and ϕ-angle restraints using simulated annealing protocols as well as NMR analysis of molecular flexibility in solution (NAMFIS) conformer deconvolution. Despite disagreement between the latter two structure analysis methodologies for shorter peptides,[18,19] the methods appear to converge in terms of structure prediction for concatenated peptides such as compound **6**. Results demonstrate (a) that selective coordination of metal ions occurs only at (i, $i + 4$) histidine positions in water and DMF, (b) that 2- and 3-α-turn mimicking modules of [Pd(en)(H*XXXH*)]$^{2+}$ can

(8) (a) Rajashankar, K. R.; Ramakumar, S.; Jain, R. M.; Chauhan, V. S. *J. Am. Chem. Soc.* **1995**, *117*, 10129. (b) Karle, I. L.; Balaram, P. *Biochemistry* **1990**, *29*, 6747.

(9) (a) Mayne, L.; Englander, S. W.; Qiu, R.; Yang, J.; Gong, Y.; Spek, E. J.; Kallenbach, N. R. *J. Am. Chem. Soc.* **1998**, *120*, 10643. (b) Albert, J. S.; Hamilton, A. *Biochemistry* **1995**, *34*, 984. (c) Butterfield, S. M.; Patel, P. R.; Waters, M. L. *J. Am. Chem. Soc.* **2002**, *124*, 9751.

(10) Jackson, D. Y.; King, D. S.; Chmielewski, J.; Singh, S.; Schultz, P. G. *J. Am. Chem. Soc.* **1991**, *113*, 9391.

(11) Cabezas, E.; Satterthwait, A. C. *J. Am. Chem. Soc.* **1999**, *121*, 3862.

(12) (a) Schievano, E.; Mammi, S.; Bisello, A.; Rosenblatt, M.; Chorev, M.; Peggion, E. *J. Pept. Sci.* **1999**, *5*, 330. (b) Bracken, C.; Gulyas, J.; Taylor, J. W.; Baum, J. *J. Am. Chem. Soc.* **1994**, *116*, 6431. (c) Phelan, J. C.; Skelton, N. J.; Braisted, A. C.; McDowell, R. S. *J. Am. Chem. Soc.* **1997**, *119*, 455. (d) Taylor, J. W.; Yu, C. *Bioorg. Med. Chem.* **1999**, *7*, 161. (e) Yu, C.; Taylor, J. W. *Tetrahedron Lett.* **1996**, *37*, 1731. (f) Zhang, M.; Wu, B.; Baum, J.; Taylor, J. W. *J. Pept. Res.* **2000**, *55*, 398.

(13) Orner, B. P.; Ernst, J. T.; Hamilton, A. D. *J. Am. Chem. Soc.* **2001**, *123*, 5382. (b) Horwell, D. C.; Howson, W.; Nolan, W. P.; Ratcliffe, G. S.; Rees, D. C.; Willems, H. M. G. *Tetrahedron* **1995**, *51*, 203.

(14) (a) Magnus, K. A.; Hazes, B.; Ton-That, H.; Bonaventura, C.; Bonaventura, J.; Hol, W. G. *Proteins* **1994**, *19*, 302. (b) Greisman, H. A.; Pabo, C. O. *Science* **1997**, *275*, 657. (c) Holland, D. R.; Hausrath, A. C.; Juers, D.; Matthews, B. W. *Protein Sci.* **1995**, *4*, 1955.

(15) (a) Hahn, M.; Wolters, D.; Sheldrick, W. S.; Hulsbergen, F. B.; Reedijk, J. *J. Biol. Inorg. Chem.* **1999**, *4*, 412. (b) Tsiveriotis, P.; Hadjiliadis, N.; Savropoulos, G. *Inorg. Chim. Acta* **1997**, *261*, 83. (c) Milinkovic, S. U.; Parac, T. N.; Djuran, M. I.; Kostic, N. M. *J. Chem. Soc., Dalton Trans.* **1997**, 2771. (d) Sovago, I. In *Biocoordination Chemistry, Coordination Equilibria in Biologically Active Systems*; Ellis Horwood: London, 1990. (e) Tsiveriotis, P.; Hadjiliadis, N. *J. Chem. Soc., Dalton Trans.* **1999**, 459. (f) Livera, C. E.; Pettit, L. D.; Battaaille, M.; Perly, B.; Kozlowski, H.; Radomska, B. *J. Chem. Soc., Dalton Trans.* **1987**, 661. (g) Agarwal, R. P.; Perrin, D. D. *J. Chem. Soc., Dalton Trans.* **1976**, 89. (h) Ueda, J.; Ikota, N.; Hanaki, A.; Koga, K. *Inorg. Chim. Acta* **1987**, *135*, 43. (i) Kozlowski, H.; Bal, W.; Dyba, M.; Kowalik-Jankowska, T. *Coord. Chem. Rev.* **1999**, *184*, 319. (j) Parac, T. N.; Kostic, N. M. *Inorg. Chem.* **1998**, *37*, 2141.

(16) (a) Ghadiri, M. R.; Fernholz, H. *J. Am. Chem. Soc.* **1990**, *112*, 9633. (b) Ghadiri, M. R.; Choi, C. *J. Am. Chem. Soc.* **1990**, *112*, 1630. (c) Ruan, F.; Chen, Y.; Hopkins, P. B. *J. Am. Chem. Soc.* **1990**, *112*, 9403. (d) Kohn, W. D.; Kay, C. M.; Sykes, B. D.; Hodges, R. S. *J. Am. Chem. Soc.* **1998**, *120*, 1124. (e) Kohtani, M.; Kinnear, B. S.; Jarrold, M. F. *J. Am. Chem. Soc.* **2000**, *122*, 12377.

(17) (a) Kelso, M. J.; Hoang, H. N.; Appleton, T. G.; Fairlie, D. P. *J. Am. Chem. Soc.* **2000**, *122*, 10488. (b) Kelso, M. J.; Hoang, H. N.; Oliver, W.; Sokolenko, N.; March, D. R.; Appleton, T. G.; Fairlie, D. P. *Angew. Chem., Int. Ed.* **2002**, *42*, 421.

(18) Snyder, J. P.; Lakdawala, A. S.; Kelso, M. J. *J. Am. Chem. Soc.* **2003**, *125*, 632−633.

(19) As with the single-turn α-helix,[18] a NAMFIS conformational analysis did not support helicity for [Pd(en)(H*ELTH*)]$^{2+}$ Lakdawala, A.; Snyder, J. P. 2003, unpublished work.

Chart 1

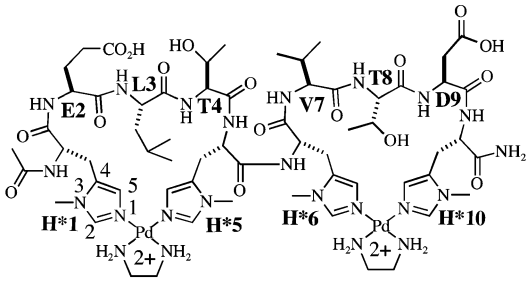

4

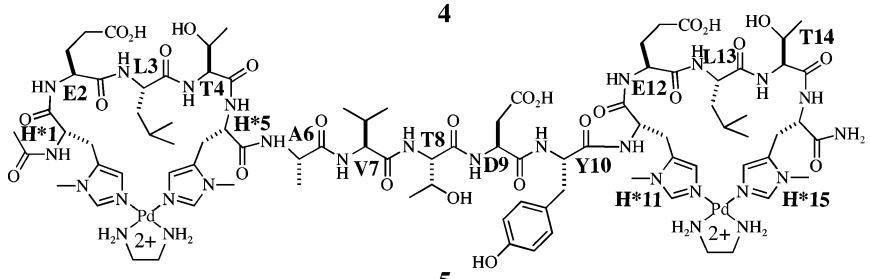

5

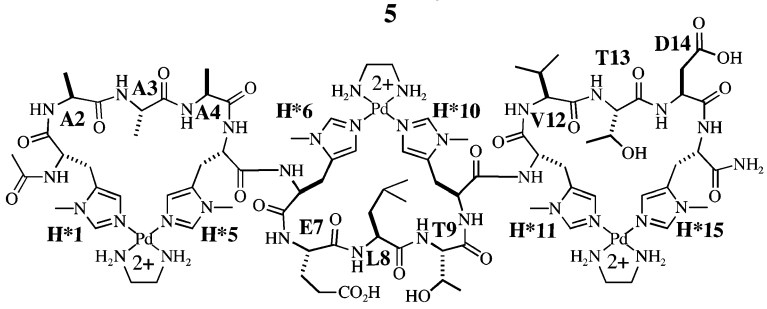

6

be incorporated within 10 and 15 residue peptides, (c) that unstructured peptides can be converted to 3- and 4-turn α-helices of macrocycles in a single step, with α-helicity being well-defined throughout the peptides including at the N- and C-termini, and (d) that there is much more structure in an aprotic solvent (DMF) than in water.

Experimental Section

General. Fmoc-N3-methyl-His-OH was obtained from Bachem AG (Switzerland). Rink amide methylbenzhydrylamine (MBHA) resin and other Fmoc-L-amino acids, (Fmoc-Ala-OH, Fmoc-Glu(O*t*Bu)-OH, Fmoc-Asp(O*t*Bu)-OH, Fmoc-Leu-OH, Fmoc-Thr(Bzl)-OH, Fmoc-Val-OH, and Fmoc-Tyr(*t*Bu)-OH), were obtained from Novabiochem (Melbourne, Australia). 2-(1*H*-Benzotriazol-1-yl)-1,1,3,3-tetramethyluronium-hexafluorophosphate (HBTU) was obtained from Richelieu Biotechnologies (Quebec, Canada). DMF-d_7 (0.7 mL ampules) was obtained from the Aldrich Chemical Co. (Milwaukee, WI). All other reagents were of peptide synthesis grade and obtained from Auspep (Melbourne, Australia).

Semipreparative reversed-phase high-performance liquid chromatography (rp-HPLC) purification of the linear peptides was performed using a Waters Delta 600 chromatograpy system fitted with a Waters 486 tunable absorbance detector with detection at 254 nm. Purification was performed by eluting with solvents A (0.1% trifluoroacetic acid (TFA) in water) and B (9:1 CH_3CN/H_2O, 0.1% TFA) on a Vydac C_{18} 250 × 22 mm (300 Å) steel-jacketed column run at 15 mL/min. Analytical rp-HPLC analyses were performed using a Waters 600 chromatography system fitted with a Waters 996 photodiode array detector and processed using Waters Millenium software. Analytical analyses were performed using gradient elutions with solvents A and B on a Vydac C_{18} 250 × 4.6 mm (300 Å) peptide and protein column run at 1.0 mL/min.

Compound Synthesis and Purification. Free peptides **1**, **2**, and **3** were prepared using manual stepwise solid-phase peptide synthesis protocols with HBTU/diisopropylethylamine (DIPEA) activation for Fmoc chemistry on Rink Amide MBHA resin (substitution 0.72 $mmol \cdot g^{-1}$, 0.25 mmol scale syntheses, 350 mg of resin). Four equivalents of Fmoc-protected amino acids, 4 equiv of HBTU, and 2 equiv of DIPEA were employed in each coupling (except for coupling of Fmoc-N3-Me-His-OH, where only 2 equiv of amino acid and HBTU were employed). Fmoc-deprotections and resin neutralization were achieved by 2 × 2 min treatments with excess 1:1 piperidine/DMF. Coupling yields were monitored by quantitative ninhydrin assay,[20] and double couplings were employed for yields below 99.8%. N-terminal acetylation was achieved by treating the fully assembled and protected peptide resins (after removal of the N-terminal Fmoc group) with a solution containing 870 μL of acetic anhydride and 470 μL of DIPEA in 15 mL of DMF (2 × 5 min treatments with enough solution to cover the resin beads). The peptides were cleaved from their respective resins, and protecting groups were simultaneously removed by treatment for 2 h at room temperature with a solution containing 95% trifluoroacetic acid (TFA):2.5% H_2O:2.5% triisopropylsilane (TIPS) (25 mL of solution per 1 g of peptide resin). The TFA solutions were filtered, concentrated in vacuo, diluted with 50% A:50% B, lyophilized, and subsequently purified by semipreparative rp-HPLC.

Ac-H*ELTH*H*VTDH*-NH_2 (1). Linear gradient from 0 to 15% B over 30 min. Yield = 25%. [R_t = 20 min.] Anal. rp-HPLC (linear gradient from 0 to 100% B over 30 min). R_t = 16.0 min. MS: [obsd $(M + 2H^+)/2$ 950.65; calcd 950.47; obsd $(M + 3H^+)/3$ 634.43; calcd 634.36].

Ac-H*ELTH*AVTDYH*ELTH*-NH_2 (2). Step gradient with 5% steps every 20 min for 1.5 h starting from 0% A. Yield = 15%. [R_t =

(20) Sarin, V.; Kent, S. B. H.; Tan, J. P.; Merrifield, R. B. *Anal. Biochem.* **1981**, *20*, 147.

58 min.] Anal. rp-HPLC (linear gradient from 0 to 100% B over 30 min). R_t = 18.6 min. MS: [obsd (M + 2H$^+$)/2 661.94; calcd 661.82; obsd (M + 3H$^+$)/3 441.96; calcd 441.82].

Ac-H*AAAH*H*ELTH*H*VTDH*-NH$_2$ (3). Linear gradient from 0 to 70% B over 30 min. Yield = 18%. [R_t = 10.5 min.] Anal. rp-HPLC (linear gradient from 0 to 100% B over 30 min). R_t = 16.4 min. MS: [obsd (M + 2H$^+$)/2 919.60; calcd 919.46; obsd (M + 3H$^+$)/3 613.74; calcd 613.67].

[Pd(en)(ONO$_2$)$_2$]. [Pd(en)Cl$_2$] was prepared according to the literature method.[21] The dichloro complex was then dissolved in water and stirred with 2.2 equiv of AgNO$_3$ in the dark at 60 °C for 2 h and then at room temperature for a further 24 h. The AgCl precipitate was removed by gravity filtration, and the filtrate was concentrated by gentle heating on a hot plate to yield a residue of [Pd(en)(ONO$_2$)$_2$] as a yellow solid (73%). Anal. Calcd for $C_2H_8N_4O_6Pd$: C, 8.27; H, 2.78; N, 19.28. Found: C, 8.25; H, 2.73; N, 18.72.

NMR Spectroscopy. Samples for NMR analysis of metallopeptide complexes **4**−**6** were prepared by separately dissolving the linear peptides **1** (6.0 mg, 4.54 μmol), **2** (6.0 mg, 3.16 μmol), and **3** (6.0 mg, 3.26 μmol) in 0.5 mL of DMF-d_7 and titrating (directly into the NMR tube) the desired number of equivalents (2, 2, and 3 equiv for **1**, **2**, and **3**, respectively) of Pd (from a stock solution of Pd(en)(ONO$_2$)$_2$: 9.48 mg, 32.6 μmol in 100 μL of DMF-d_7). Titrations in DMF were monitored by recording 1D ^{1}H-spectra immediately after Pd addition. Samples in water were prepared by dissolving the linear peptides **1** (4.0 mg, 3.03 μmol), **2** (4.0 mg, 2.11 μmol), and **3** (4.0 mg, 2.17 μmol) in 0.5 mL of H$_2$O/D$_2$O (9:1) and titrating (directly into the NMR tube) the desired number of equivalents (2, 2, and 3 equiv for **1**, **2**, and **3**, respectively) of Pd (from a stock solution of Pd(en)(ONO$_2$): 1.5 mg, 5.00 μmol in 100 μL of H$_2$O/D$_2$O (9:1)). The solutions were adjusted from pH 2 to pH 4.2−4.4 using 0.01 M NaOH and 0.01 M HNO$_3$.

1D and 2D ^{1}H NMR spectra were recorded on either a Bruker ARX-500 or Bruker Avance DMX-750 spectrometer. 2D ^{1}H-spectra were recorded in phase-sensitive mode using time-proportional phase incrementation for quadrature detection in the $t1$ dimension.[22a] The 2D experiments included TOCSY (standard Bruker mlevtp or mlevph pulse programs) and NOESY (standard Bruker noesytp or noesyph pulse programs). TOCSY spectra were acquired over 6887 Hz with 4096 complex data points in F_2, 512 increments in F_1, and 16 scans per increment. NOESY spectra were acquired over 6887 Hz with 4096 complex data points in F_2, 512 increments in F_1, and 48 scans per increment. TOCSY spectra were acquired with an isotropic mixing time of 80 ms. For TOCSY and NOESY experiments in 90% H$_2$O:10% D$_2$O, water suppression was achieved using a modified WATERGATE sequence.[22b] For 1D ^{1}H NMR spectra in water, the water resonance was suppressed by low-power irradiation during the relaxation delay (1.5 s). Spectra were processed using XWINNMR (Bruker, Germany) software. The $t1$ dimensions of all 2D spectra were zero-filled to 1024 real data points with 90° phase-shifted QSINE bell window functions applied in both dimensions followed by Fourier transformation and fifth-order polynomial baseline correction. ^{1}H chemical shifts were referenced to the residual CHO proton in DMF-d_7 (δ 8.01 ppm) and to HDO (δ 4.80 ppm) or 1,4-dioxane (δ 3.70 ppm) in water. $^3J_{NHC\alpha}$ coupling constants were measured from high-resolution 1D spectra.

^{15}N NMR spectra (40.5 MHz) were obtained at 298 K using a DEPT pulse sequence on a Bruker AMX-400 spectrometer fitted with a 5-mm broad-band tunable probe. ^{15}N chemical shifts were referenced to the $^{15}NH_4^+$ signal (0.0 ppm) from 5 M ($^{15}NH_4$)$_2$SO$_4$ in 1 M H$_2$SO$_4$ in a coaxial capillary.

Mass Spectrometry. Positive ion electrospray mass spectra (ESI-MS) were recorded on a Micromass (Manchester, U.K.) LCT-QTOF mass spectrometer. Samples for analysis of the metallopeptide complexes **4**−**6** were prepared in a manner identical to those used for NMR analysis (see above), except for the use of unlabeled DMF in place of DMF-d_7. The DMF solutions of the complexes were injected directly into the injector port of the MS and carried to the source by a 1:1 mixture of solvents A and B (solvent A = 100% H$_2$O with 0.1% formic acid; solvent B = 90% CH$_3$CN:10% H$_2$O with 0.1% formic acid) at a flow rate of 100 μL·min^{-1}. The mass spectra were recorded and processed with Masslynx software (version 3.5). The following isotopic distribution diagnostic for Pd was used in the analysis: 1.0% ^{102}Pd, 11.1% ^{104}Pd, 22.3% ^{105}Pd, 27.3% ^{106}Pd, 26.5% ^{108}Pd, and 11.8% ^{110}Pd. To simplify the assignment of peaks, the m/z values quoted in the text refer to the average mass of each peak cluster. These average masses were calculated from the average molecular weights (M) derived from the molecular formula. For example, in complex **4**, the molecular formula ($C_{62}H_{103}N_{23}O_{17}Pd_2$) produces an average molecular weight M = 1655.49 amu. Therefore the m/z = (M/4) peak was assigned a value of 1655.49/4 = 413.9 amu. The m/z = (M − H$^+$)/3 peak was assigned a value of (1655.59−1.00794)/3 = 551.5 amu.

NMR Structure Calculations by Simulated Annealing and Energy Minimization. Structural Restraints. The distance restraints used in calculating the solution structures for **4**−**6** in DMF-d_7 were derived from NOESY spectra (recorded at 298 K for **4** and **5** and 318 K for **6**) using mixing times of 250 ms for **5** or 350 ms for **4** and **6** in water, and 300 ms for **5** and 400 ms for **4** and **6** in DMF. NOE cross-peak volumes were classified manually as strong (upper distance constraint ≤2.7 Å), medium (≤3.5 Å), weak (≤5.0 Å), and very weak (≤6.0 Å), and standard pseudoatom distance corrections[23] were applied for nonstereospecifically assigned protons. To address the possibility of conformational averaging, intensities were classified conservatively, and only upper distance limits were included in the calculations to allow the largest possible number of conformers to fit the experimental data. Backbone dihedral angle restraints were inferred from $^3J_{NHC\alpha}$ coupling constants. For $^3J_{NHC\alpha} \leq 6$ Hz, ϕ was restrained to $-65 \pm 25°$. No restraints were included for residues with $6 \leq \phi \leq 8.5$ Hz because of the problem of multiple solutions to the Karplus equation over this range.[24] No residues in complexes **4**, **5**, or **6** displayed $^3J_{NHC\alpha}$ coupling constants >8.5 Hz. No evidence for cis-peptide amides (i.e., no CH_α−CH_α i, i + 1 NOEs) was present in the NOESY spectra for the complexes, and therefore all ω-angles were set to trans (ω = 180°). Structures were calculated without any explicit hydrogen bond restraints to prevent structure biasing.

Structure Calculations. Three-dimensional structures of the peptide backbones in complexes **4**−**6** were calculated (without Pd(en)$^{2+}$) using a dynamic simulated annealing and energy minimization protocol in the program X-PLOR 3.851. Starting structures with randomized ϕ and ψ angles and extended side chains were generated using an ab initio simulated annealing protocol.[25] The calculations were performed using the standard force field parameter set (PARALLHDG.PRO) and topology file (TOPALLHDG.PRO) in X-PLOR, which included in-house modifications to account for histidine N3-methyl groups. Refinement of the structures was achieved using the conjugate gradient Powell algorithm with 1000 cycles of energy minimization and a refined force field based on the program CHARMm[26] The final 20 structures chosen to represent the lowest energy conformation for each of **4**−**6** contained no distance violations ≥0.2 Å and no dihedral violations ≥2°. Structures were displayed in Insight II (version 2000.1, Accelrys, San Diego, CA).

Deconvolution of the NMR Average Structure by NAMFIS Analysis. Conformational analysis for tripalladated **6** was accomplished

(21) McCormack, J. B.; Jaynes, E. N.; Kaplan, R. I. *Inorg. Synth.* **1972**, *13*, 216.
(22) (a) Marion, D.; Wüthrich, K. *Biochem. Biophys. Res. Commun.* **1983**, *113*, 967. (b) Piotto, M.; Saudek, V.; Sklenar, V. *J. Biomol. NMR* **1992**, *2*, 661−665.
(23) Wüthrich, K.; Billeter, M.; Braun, W. *J. Mol. Biol.* **1983**, *169*, 949.
(24) Mierke, D. F.; Huber, T.; Kessler, H. *J. Comput.-Aided. Mol. Des.* **1994**, *8*, 29−40.
(25) Nilges, M.; Gronenborn, A. M.; Brünger, A. T.; Clore, G. M. *Protein Eng.* **1988**, *2*, 27.
(26) Brooks, B. R.; Bruccoleri, R. E.; Olafson, B. D.; States, D. J.; Swaminathan, S.; Karplus, M. *J. Comput. Chem.* **1983**, *4*, 187.

by initially breaking the problem into three smaller components. Thus, each of the cyclic peptides Pd^{2+}[H*AAAH*] (**7**), Pd^{2+}[H*ELTH*] (**8**), and Pd^{2+}[H*VTDH*] (**9**) was subjected to a 180 000-step Monte Carlo conformational search with AMBER*/GBSA/H2O and a 7 kcal/mol energy window in MacroModel 6.5. AMBER* parameters suitable for planar, tetravalent Pd^{2+} in the present molecular environment were taken from our previous work.[18] This provided 1835, 1345, and 1270 AMBER*-optimized conformers for **7**−**9**, respectively. Each conformer set was supplemented with two helical conformations. The first was generated by constrained torsional optimization to give an ideal α-helical structure with two *i*, *i* + 4 hydrogen bonds for each metalated cyclic pentapeptide. The second conformer was obtained through unconstrained optimization of the α-helical structure, resulting in a 3_{10}-helix for both Pd^{2+}[H*AAAH*] and Pd^{2+}[H*ELTH*], and a preservation of an ideal α-helical conformation for Pd^{2+}[H*VTDH*]. The individual conformational families of 1837, 1347, and 1272 members were then subjected to a NAMFIS analysis[27,28] employing the intrapeptide NOEs and three-bond coupling constants ($^3J_{NHC\alpha H}$) applicable to that peptide in the NMR spectrum of **6** in both DMF-d_6 and D_2O. The goodness-of-fit is expressed as the sum of square differences (SSD) between the measured and modeled variables. A detailed discussion of this statistic can be found in previous reports.[27,28] Tables 2 and 3 summarize the quantities combined by NAMFIS during the various conformational deconvolutions. NMR parameters describing interactions between the cyclic peptides that are present in the tripalladated peptide **6** were ignored during this stage of analysis.

For analysis of the tripalladated peptide **6**, the complete set of NMR observables in the two solvents were employed by NAMFIS, but the set of conformers was limited to six structures. The first four structures, which are helical in nature and common to the DMF-d_6 and D_2O analyses, were (1) an ideal α-helical conformation constructed by merging the individual α-helical Pd-pentapeptides followed by distance and torsional constrained AMBER* optimization of the trimer to ensure α-helical structure throughout (**H$_{DMF}$** and **H$_{D2O}$**, Figure 11a), (2) a helical conformation in which the individual Pd-pentapeptides are helical, but the connections between them correspond to a 3_{10}-helix (**H′$_{DMF}$** and **H′$_{D2O}$**). This structure was obtained by geometry optimization with constraints placed only on the cyclic peptides **7**−**9** and not on their interconnections (Figure 11b**)**, (3) a helical conformation from unconstrained optimization of **H$_{DMF}$**/**H$_{D2O}$** to give **H″$_{DMF}$** and **H″$_{D2O}$**, respectively; these structures are very similar to **H$_{DMF}$**/**H$_{D2O}$** but the peptide backbone for fragment **9** (Pd^{2+}[H*VTDH*]) has become a 3_{10}-helix (Figure 11c), and (4) a conformation derived from unconstrained optimization of **H′$_{DMF}$**/**H′$_{D2O}$** to give **H‴$_{DMF}$**/**H‴$_{D2O}$**, a mixture of α- and 3,10-helices, but with irregular distribution of the helix types along the tripeptide length (Figure 11d).

The remaining two tripeptide conformations differ for the two solvents, since the components are taken from the separate preliminary NAMFIS evaluations of **7**−**9** (see below). Thus, conformation 5 is a combination of the top conformers derived from the three individual NAMFIS Pd-pentapeptide deconvolutions. In DMF-d_6, the component represented by **7** is an ideal α-helix; **8**, a γ-turn; and **9**, a loop structure (**N$_{DMF}$**, Figure 12a**)**. In D_2O, the corresponding fragments are a β-turn, an ideal α-helix, and an alternative loop structure (**N$_{D2O}$**, Figure 12b**)**. In each case, the conformations represent 40−95% of the total population of the peptide in solution. Conformation 6 is the top NAMFIS conformation from 5 optimized without constraints. For DMF-d_6, this structure is the least organized of the six and characterized by only three hydrogen bonds, none of which are found in the HELTH fragment (**N′$_{DMF}$**, Figure 12c). In D_2O, the conformer sustains five hydrogen bonds, one of which is a side-chain backbone interaction (**N′$_{D2O}$**, Figure 12d**)**. The structure represents a modest reorganization of hydrogen bonds and a significant variation in backbone torsions relative to **N$_{D2O}$**.

Each of the eight metalated tripeptide structures are depicted with hydrogen bonds in Figures 11 and 12. This small dataset allows evaluation of how well the ideal α-helix conformation competes against alternative structures with diminishing helical character in the NAMFIS framework. The situation is not equivalent to a conformer deconvolution based on a complete or extensive search of conformational space as was performed for the individual pentapeptides **7**−**9**. Compound **6** is simply too complex to explore all important aspects of its conformational surface. However, the approach does bypass the assumption associated with a single target conformation in the simulated annealing exercise.

Circular Dichroism Spectra. CD measurements were performed using a Jasco model J-710 spectropolarimeter, which was routinely calibrated with (1*S*)-(+)-10-camphorsulfonic acid. Each metallopeptide complex was dissolved in water (concentration 20−50 μM) at different pH values ranging from 2 to 7. Temperature control was achieved using a Neslab RTE-111 circulating water bath. Spectra were recorded at 298 K, with a 0.1-cm Jasco quartz cell over the wavelength range 300−190 nm at 50 nm/min with a bandwidth of 1.0 nm, response time of 2 s, resolution step width of 0.1 nm, and sensitivity of 20 M/deg. Each spectrum represents the average of five scans with smoothing to reduce noise.

Results and Discussion

1D ^{1}H NMR Spectroscopy. Formation of complexes **4**−**6** was identified by monitoring the reactions of [Pd(en)(NO_3)$_2$] with **1**−**3**, respectively, in DMF-d_7 at 298 K by 1D ^{1}H NMR spectroscopy. Aliquots of a stock solution of [Pd(en)(NO_3)$_2$] in DMF-d_7 were titrated directly into NMR tubes containing solutions of free peptides **1**−**3** in DMF-d_7. For peptides **1** and **2**, addition of <2 equiv of Pd produced complex spectra (Figures S1 and S2, Supporting Information), consistent with the presence of multiple species, but upon reaching 2.0 equiv, the complex myriad of signals rapidly converged to a single set of resonances, indicating just one thermodynamically stable metallopeptide product.

Similarly, titration of **3** with [Pd(en)(NO_3)$_2$] in DMF-d_7 gave a complex mixture of species (Figure 1) with up to 3.0 equiv of Pd^{2+}, whereupon a single resonance set for just one species (**6**) was observed. However, the temperature needed to be raised to 318 K to ensure complete reaction after 3.0 equiv of Pd^{2+}. During this conversion, resonances for **6** in the amide/aromatic region of the spectrum (∼6.6−9.5 ppm) were broadened and significantly overlapped, but on completion of the reaction (minutes at 318 K), the amide and aromatic resonances of **6** became sharper and fully resolved (Figure 1).

Mass Spectrometry. Although the 1D- (above) and 2D- (below) ^{1}H NMR spectra provided very strong evidence for the identity and structures of complexes **4**−**6**, we sought confirmation for their respective molecular masses from mass spectrometry. Pd contains six naturally occurring isotopes, so that each Pd species in mass spectra exhibits a complex cluster of isotope peaks. The separation between isotopes can be used to establish the charge state of the parent ion. For a 1+ ion, the isotopes are separated by 1 amu, 0.5 amu for a 2+ ion, 0.33 amu for a 3+ ion, etc. Acquiring positive ion electrospray mass spectra of peptides usually involves protonating some basic species, such as a free amine or amide, to generate a detectable ion. However, complexes **4**−**6** already contain 4+, 4+, and 6+ charges due to the presence of 2 or 3 Pd^{2+} ions and thus do not

(27) Cicero, D. O.; Barbato, G.; Bazzo, R. *J. Am. Chem. Soc.* **1995**, *117*, 1027−1033.
(28) Nevins, N.; Cicero, D.; Snyder, J. P. *J. Org. Chem.* **1999**, *64*, 3979−3986.

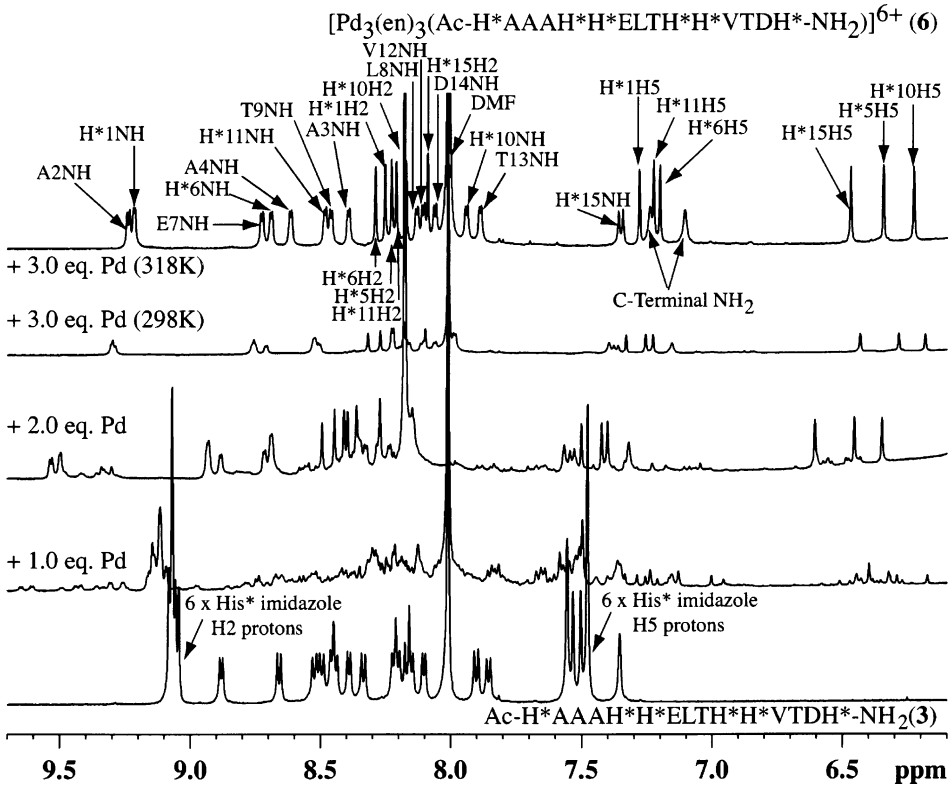

Figure 1. ^{1}H NMR monitored titration (298 K) of free peptide Ac-H*AAAH*H*ELTH*H*VTDH*-NH_2 (**3**) with [Pd(en)$(NO_3)_2$] in DMF-d_7. Only amide NH regions are shown for clarity. Adding <3.0 equiv of Pd^{2+} gave multiple species, but 3.0 equiv and an elevated temperature (318 K) produced one species, **6**. See Chart 1 for numbering.

Table 1. Summary of Mass Spectral Data for Complexes **4**−**6**

	complexes and observed ions (*m*/*z*)		
assignments[a] (*m*/*z*)	**4**[b]	**5**[c]	**6**[d]
[M]/4	413.9 (0.24)	558.3 (0.25)	
[M − H^+]/3	551.5 (0.33)	744.0 (0.33)	
[M − $2H^+$]/2	826.7 (0.50)	1115.6 (0.49)	
[M − H^+]/5			478.1 (0.20)
[M − $2H^+$]/4			584.9 (0.25)
[M − $3H^+$]/3			779.5 (0.34)

[a] Molecular ions for each charge state corresponding to observed ions. Numbers in parentheses are average peak separations in clusters and identify ion charge states. [b] MW = 1655.49. [c] MW = 2233.12. [d] MW = 2341.61.

require protonation to be observed. One might therefore expect to see *m*/*z* = (M/4) ions for **4** and **5** and *m*/*z* = (M/6) ion for **6**. Figure 2a,b (and Table 1) indeed show the *m*/*z* = (M/4) ions for both **4** and **5**.

These were not the only species; two additional peaks were observed in each spectrum. The isotope separations within these extra peaks corresponded to 3+ and 2+ ions (Table 1), and for both complexes, the *m*/*z* ratios for the two extra peaks corresponded to (M − H^+)/3) and (M − $2H^+$)/2) ions. When the three ions in each spectrum were deconvoluted, the reconstructed molecular mass (using Masslynx software, insets to Figure 2a,b) and isotope distribution corresponded to the theoretical 1+ molecular ion mass and distribution calculated for the molecular formulas of **4** and **5**. This confirmed that all three ions corresponded to the expected different charge states for each of the two complexes **4** and **5**. We suspect that the 3+ and 2+ ions arose from deprotonation of the Glu and Asp side chains in the mass spectrometer.

The mass spectrum for **6** was different in that the expected *m*/*z* = (M/6) ion was not observed. Only ions resulting from one, two, and three deprotonations, (M − H^+)/5, (M − $2H^+$)/4, and (M − $3H^+$)/3, respectively, were observed. When these three ions were deconvoluted in a molecular mass reconstruction (Figure 2c inset), the resultant mass and isotope distribution corresponded to the expected theoretical 1+ molecular ion for $C_{87}H_{148}N_{34}O_{22}Pd_3$, confirming that all three ions were simply different charge states of **6**.

Two-Dimensional ^{1}H NMR Spectroscopy. TOCSY Spectra. 2D-TOCSY spectra were used to identify spin systems corresponding to individual amino acids in the products of the three reactions. The presence of a single peptidic species in DMF-d_7 was suggested in each of **4**−**6** (Figures S3−S5, Supporting Information), since only 10 spin systems were present for **4** and 15 spin systems for **5** and **6**. Chemical shift assignments for **4**−**6** are recorded in Tables S3−S5 of the Supporting Information.

NOESY Spectra. The presence of a single product in each reaction was confirmed by employing the sequence-specific resonance assignment method of Wüthrich.[29] In the 750 MHz NOESY spectra of putative reaction products **4**−**6**, connectivity could be traced throughout only a single network of alternating intraresidue NH−Hα cross-peaks and sequential Hα−NH (*i*, *i* + 1) and HN−HN (*i*, *i* + 1) cross-peaks. No other sequential connectivities were observed, and all of the other cross-peaks in each spectrum could be assigned to just one species. Importantly, long range cross-peaks were observed between the imidazole protons of metal-bound His* residue pairs in each

(29) Wüthrich, K. *NMR of Proteins and Nucleic Acids*; Wiley-Interscience: New York, 1986.

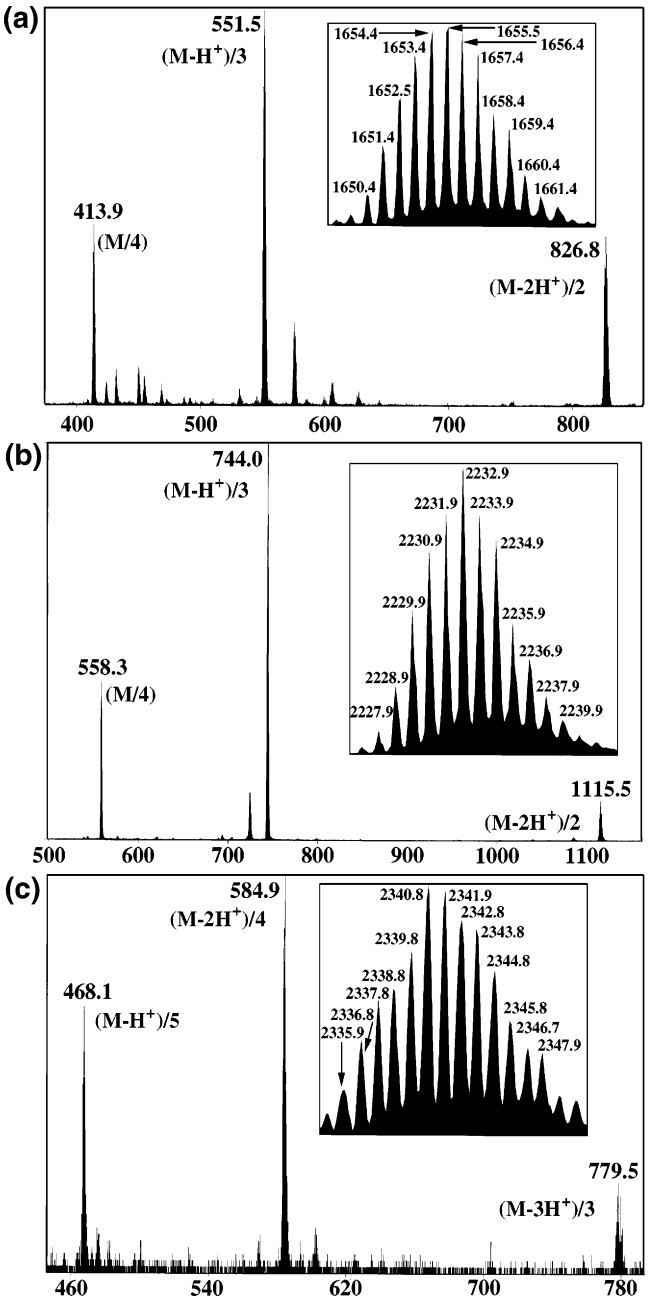

Figure 2. Electrospray mass spectra for complexes (a) **4**, (b) **5**, and (c) **6**. Insets show deconvoluted M^{1+} ions and isotopic distributions calculated for each complex from observed ions. Each deconvoluted ion cluster corresponds to the theoretical cluster calculated from the molecular formula of **4**, **5**, or **6**.

complex, unambiguously revealing the Pd binding sites. None of these NOEs were present in the respective free peptides. A NOESY spectrum highlighting these important NOEs for **6** in DMF-d_7 is shown in Figure 3, while NOESY spectra for **4** and **5** (Figures S6 and S7) and free peptides **1**−**3** (Figures S8−S10) in DMF-d_7 are presented in the Supporting Information.

CH_α Chemical Shifts. The CH_α proton chemical shifts for residues in peptides and proteins are highly sensitive to structural effects. For residues involved in β-strand or extended conformations, these chemical shifts tend to appear $>+0.1$ ppm downfield relative to their shifts when involved in random coils. For residues involved in α-helices, the CH_α shifts move upfield by similar amounts.[30] NOESY spectra (500 MHz) for free peptides **1**−**3** in DMF-d_7 (Figures S8−S10, Supporting Information) showed only intraresidue and sequential cross-peaks, with no medium or long-range cross-peaks, suggesting that **1**−**3** predominantly adopt randomly extended conformations in this solvent. Chemical shifts for CH_α protons of free peptides **1**−**3** therefore approximate random coil values for the constituent amino acids in DMF-d_7 and can be compared directly with those of the corresponding complexes **4**−**6** as a measure of structure induction. Figure 4 shows that CH_α chemical shifts for **4**−**6** (except A3 and A4 of **6**) are >0.1 ppm upfield of those for corresponding free peptides **1**−**3**, supporting α-helical structures for **4**−**6**. Upfield shifts of <0.1 ppm for A3 and A4 of **6** may reflect some helicity within the AAA segment of **3**, a feature supported by $^3J_{NHCH\alpha}$ coupling constant data below, as the helix-stabilizing propensity of Ala-containing and poly-Ala sequences is well-known.[31] Importantly, this helix induction is not due to aggregation as reflected by the fact that the upfield CH_α proton chemical shifts are independent of concentration, as shown for **4** versus **1** in DMF-d_7 at 0.1, 0.5, 1.0, and 10 mM concentrations (Figure S12, Supporting Information), and CD spectra were also unchanged for 100 μM and 30 μM for **4** in water.

$^3J_{NHCH\alpha}$ Coupling Constants. The magnitude of the $^3J_{NHCH\alpha}$ coupling constants observed for each residue in peptides (and proteins) is dependent upon the ϕ-angles (according to the Karplus equation)[29,32] and therefore on local conformations in the polypeptide chains. Residues involved in secondary structures including β-sheets and α-helices can be identified from these coupling constants, since $^3J_{NHCH\alpha}$ values fall in the range of 4−6 Hz ($-70 < \phi < -30$) for α-helices, 8−10 Hz ($-150° < \phi < -90°$) for β-sheet conformations, and 6−8 Hz for random coil conformations.[33] A series of three or more coupling constants <6 Hz is usually taken as evidence for helical structure.[34]

Free peptides **1** and **2** are almost devoid of coupling constants indicative of structure (Figure 5 and Table S1 of Supporting Information), supporting their assigned random coil conformations. Upon complexation with 2 equiv of Pd(II) to form **4** and **5**, respectively, the $^3J_{NHCH\alpha}$ coupling constants for every residue except H*10 of **4** were lowered to ≤ 6 Hz, consistent with these metallopeptides adopting α-helical conformations. The free peptide **3** exhibited only random coil values for most residues, but the AAA residues displayed low coupling constants (suggesting some helicity within this segment). Upon complexation of **3** with 3 equiv of Pd(II) to give **6**, all residues (except H*15) displayed low $^3J_{NHCH\alpha}$ values consistent with helical induction.

Amide Proton Temperature Coefficients. The magnitude of temperature dependence of the chemical shift for an amide NH is generally accepted as a measure of the degree to which it is protected from solvation, most often due to hydrogen bonding.[35] For peptides, temperature coefficients ($\Delta\delta/T$) $\leq 3-4$ ppb/K are consistent with involvement in an intrachain hydrogen bond such as in an α-helix or β-sheet. Non-hydrogen-bonded

(30) (a) Wishart, D. S.; Sykes, B. D.; Richards, F. M. *J. Mol. Biol.* **1991**, *222*, 311 (b) Wishart, D. S.; Sykes, B. D.; Richards, F. M. *Biochemistry* **1992**, *31*, 1647.
(31) Wojcik, J.; Altmann, K.-H.; Scheraga, H. A. *Biopolymers* **1990**, *30*, 121.
(32) Karplus, M. J. *J. Am. Chem. Soc.* **1963**, *85*, 2870.
(33) Pardi, A.; Billeter, M.; Wuthrich, K. J. *J. Mol. Biol.* **1984**, *180*, 741.
(34) Dyson, H. J.; Wright, P. E. *Annual Review of Biophysics and Biophysical Chemistry* **1991**, *20*, 519.
(35) (a) Kessler, H. *Angew. Chem., Int. Ed. Engl.* **1982**, *21*, 512. (b) Dyson, H. J.; Cross, K. J.; Houghten, R. A.; Wilson, I. A.; Lerner, R. A. *Nature* **1985**, *318*, 480.

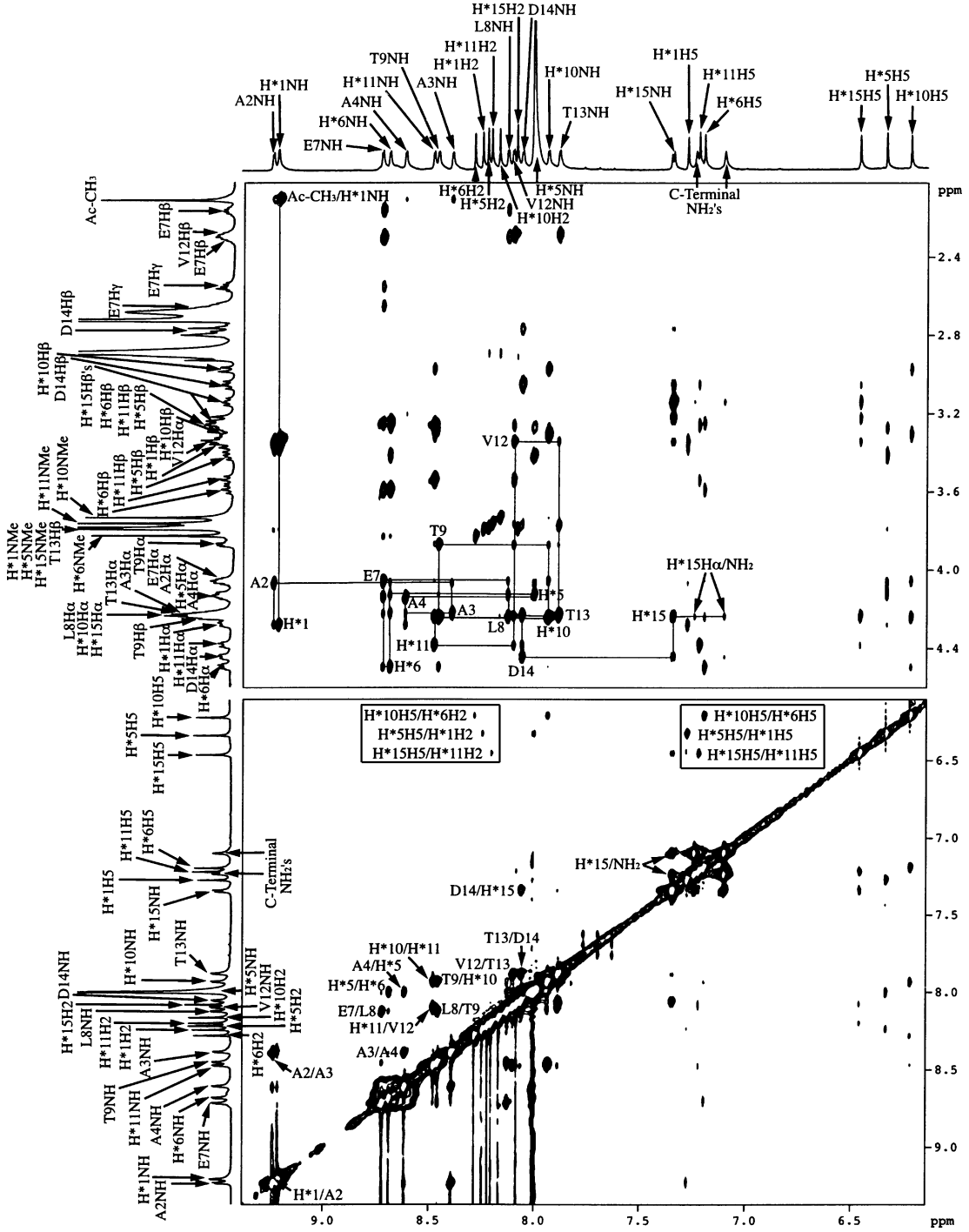

Figure 3. Sections of 750 MHz NOESY spectrum for **6** (DMF-d_7, 318 K, mixing time 400 ms). Cross-peaks are labeled by one-letter amino acid codes and by residue numbers in **6**. Top: Sequential connectivity for **6** (solid line) showing intraresidue NH−CH_α cross-peaks. Bottom: Amide NH−NH region. Cross-peaks also labeled for specific proton (e.g., H*5H5/H*1H2 = His*5-H5 to His*1-H2 and A2NH/A3NH = Ala2-NH to Ala3-NH). Long-range cross-peaks between imidazole protons of metal-bound H* residues are highlighted with boxes. See Chart 1 for numbering.

peptide NHs exposed to solvent tend to display higher $\Delta\delta/T$ values. Free peptides **1**−**3** hardly show any amide proton temperature coefficients ≤3−4 (Figure 5 and Supporting Information), consistent with their assigned random conformations. In contrast, the majority of amide protons in the metallopeptides **4**−**6** display values in this range, consistent with their involvement in multiple C═O(i) → NH(i + 4) hydrogen bonds that stabilize α-helices.

NOE Distance Information. The presence of NOE cross-peaks in 2D-NOESY spectra of peptides usually provides the most convincing evidence of structure in solution, since they are the least subject to factors that often complicate the interpretation of other spectral data.[36] Importantly, they allow conformational analysis on a per residue basis. Summaries of the sequential and medium range NOE information for metallopeptide complexes **4**−**6** in DMF are presented in Figure 5. Residues involved in α-helices are connected throughout by

(36) (a) Wüthrich, K.; Billeterm, M.; Braun, W. *J. Mol. Biol.* **1984**, *180*, 715. (b) Bradley, E. K.; Thomason, J. F.; Cohen, F. E.; Kosen, P. A.; Kuntz, I. D. *J. Mol. Biol.* **1990**, *215*, 607.

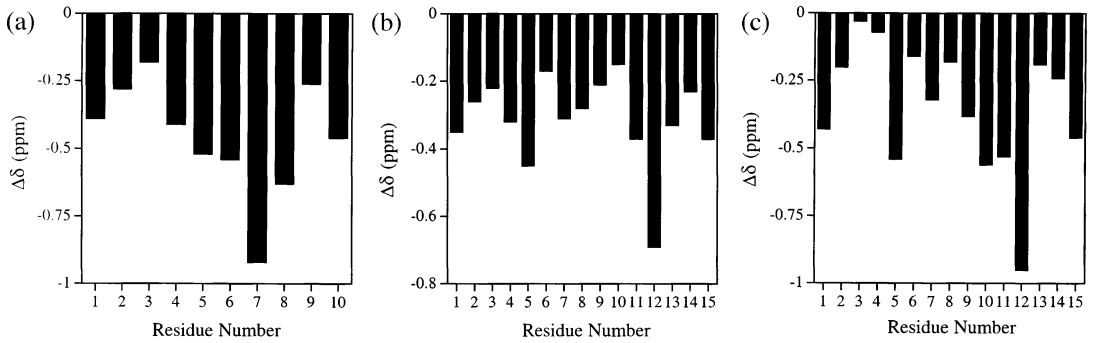

Figure 4. Upfield CH_α chemical shifts in DMF-d_7 for (a) **4** relative to **1**, (b) **5** relative to **2**, and (c) **6** relative to **3**. Negative $\Delta\delta$ values are typical of α-helicity.[26]

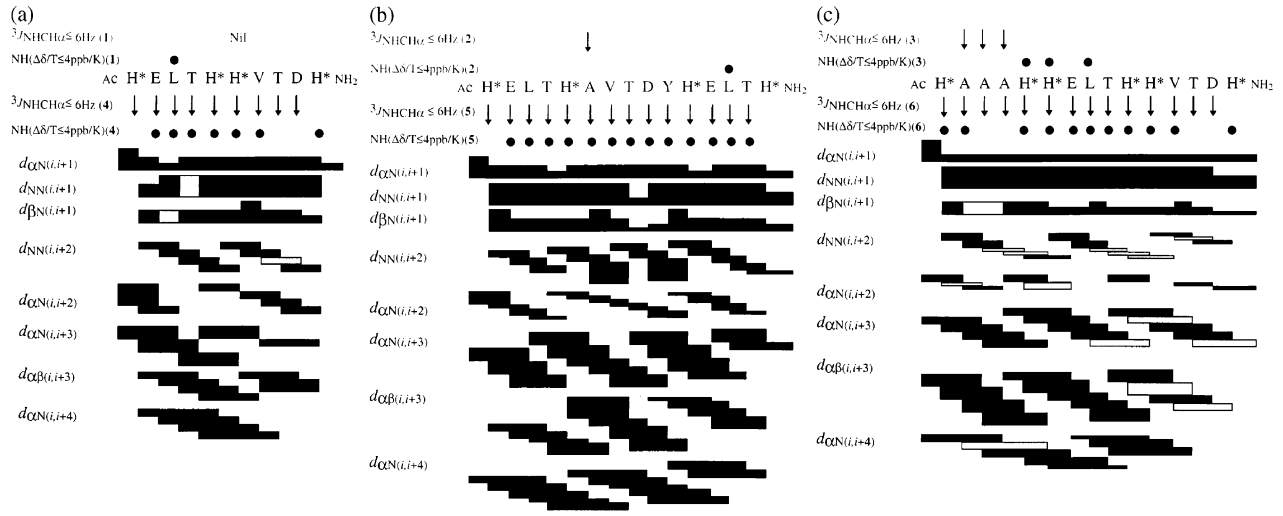

Figure 5. Summary of coupling constants $^3J_{NHC\alpha}$ (≤6 Hz shown by ↓), amide NH temperature coefficients $\Delta\delta/T$ (≤4 ppb/K shown by ●), and NOE correlations (sequential and medium range, gray bars indicate spectral overlap) for metallopeptides **4**−**6** in DMF-d_7. Coupling constants and temperature coefficients for corresponding free peptides (**1**−**3**) are shown above peptide sequences for comparison.

short $d_{\alpha N}(i, i + 1)$, $d_{NN}(i, i + 1)$, $d_{\alpha N}(i, i + 3)$, $d_{\alpha N}(i, i + 4)$, and $d_{\alpha\beta}(i, i + 3)$ distances and to a lesser extent by $d_{\alpha N}(i, i + 2)$ distances.[36a] Figure 5 shows that NOE cross-peaks corresponding to these short distances dominate the NOESY spectra of complexes **4**−**6**, the $(i, i + 3)$, and especially $(i, i + 4)$ correlations, providing very strong evidence of α-helical structures for **4**−**6**.

Solution Structures in DMF-d_7 by Simulated Annealing. Calculating 3D solution structures for short peptides from NMR-derived interproton distances and torsion angle restraints is often perilous because it assumes the existence of a single set of related conformations. Single conformations are normal for globular proteins because numerous electrostatic, hydrophobic, and hydrogen-bonding interactions provide extensive conformational stabilization; therefore, standard simulated annealing[37] and distance geometry[38] protocols are ideal methods for revealing their structure. Short peptides, on the other hand, have few of these stabilizing interactions and consequently tend to exist as ensembles of rapidly interconverting, low-energy conformers. Because NMR parameters are collected as time- and ensemble-averaged quantities, the NOE and *J*-couplings for most peptides tend to correspond only to population-weighted averaged values, and single conformations calculated from such data may not necessarily reflect the overall solution structure, unless that conformation exists with a highly predominant statistical weight.[39]

As always, there are population-weighted averages of conformations for metallopeptides **4**−**6** but additional constraints, imposed by the two (for **4** and **5**) and three (for **6**) modules of $[Pd(en)(H^*XXXH^*)]^{2+}$, which adopt stable helical turns on their own,[17] are expected to significantly limit conformational freedom compared with free peptides, leading to only one or a few stable conformations. Indeed, the combined NMR data (CH_α chemical shifts, $^3J_{NHC\alpha}$ coupling constants, VT-NMR data, NOE observations) overwhelmingly point to a predominance of α-helical conformations for **4**−**6**, and therefore, the calculation of NMR-derived solution structures is well-justified here.

Structures for **4**−**6** in DMF-d_7 were calculated from the following NMR-derived restraints. For **4**, 234 NOE distance restraints (105 intraresidue, 60 sequential, 69 medium range $i \rightarrow i + 2$, $i \rightarrow i + 3$, or $i \rightarrow i + 4$) and 9 backbone ϕ-dihedral angle restraints inferred from $^3J_{NHC\alpha}$ coupling constants were used. For **5**, 291 NOEs (109 intraresidue, 75 sequential, 107 medium range) and 14 ϕ-dihedral angles were used. For **6**, 279 NOEs (124 intraresidue, 72 sequential, 83 medium range) and

(37) Nilges, M.; Clore, M.; Gronenborn, A. *FEBS Lett.* **1998**, *239*, 129.
(38) (a) Havel, T. F.; Wüthrich, K. *Bull. Math. Biol.* **1984**, *46*, 673. (b) Braun, W.; Go, N. *J. Mol. Biol.* **1985**, *186*, 611.
(39) (a) Jardetsky, O. *Biochim. Biophys. Acta* **1980**, *621*, 227. (b) Van Gunsteren, W. F.; Brunne, R. M.; Gros, P.; van Schaik, R. C.; Schieffer, C.; Torda, A. E. *Methods Enzymol.* **1994**, *239*, 619. (c) Nikiforovich, G. V.; Kövér, K. E.; Zhang, W.-J.; Marshall, G. R. *J. Am. Chem. Soc.* **2000**, *122*, 3262−3273.

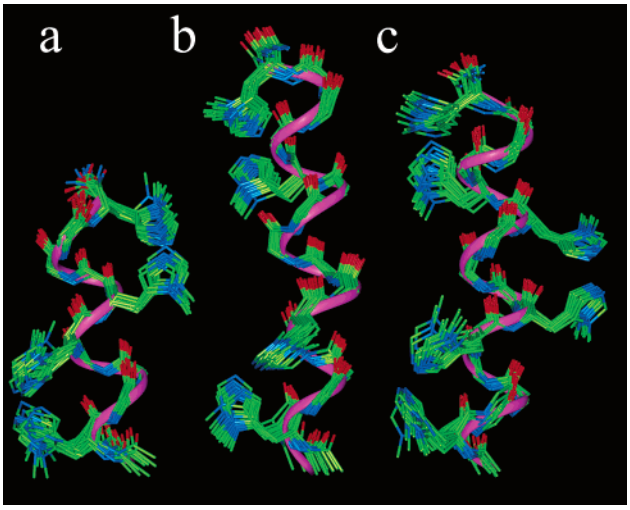

Figure 6. Backbone superimposition of the 20 lowest energy calculated solution structures for (a) **4** (av backbone pairwise rmsd 0.37 Å), (b) **5** (av backbone pairwise rmsd 0.46 Å), and (c) **6** (av backbone pairwise rmsd 0.73 Å); N-termini at base of figure. Only side chains of Pd-bound His* residues are displayed, and lowest energy conformers are indicated (purple ribbon).

14 ϕ-dihedral angles were used (see Table S7, Supporting Information). The structures were calculated in XPLOR[40] using a dynamic simulated annealing protocol in a geometric force field and were energy-minimized using a modified CHARMm[26] force field. No explicit hydrogen bond restraints were included in the structure calculations, even though the temperature-independent amide NHs strongly support multiple H-bonds, to prevent exclusion of any non-α-helical H-bonded conformers (e.g., 3_{10}-helices) should they fit the data.

The resulting structures (calculated without $Pd(en)^{2+}$) clearly identified which i, $i + 4$ His* residue pairs in each of **4**−**6** were correctly oriented for coordination to Pd(II). In the final calculations, the N1 nitrogens of these metal-bound His* residue pairs were constrained to within an upper distance of 2.7 Å of each other, which was the expected separation between nitrogens in a square planar complex with Pd−N bond lengths of 1.90 Å.[41] The calculated solution structures for **4**−**6** in DMF are displayed in Figure 6 and are all clearly very close to idealized α-helices along their entire lengths with little fraying even at their N- and C-termini.

Solution Structures for 4−6 in Water. Peptides **1**−**3**, dissolved in H_2O/D_2O (9:1), were also reacted in NMR tubes at 298 K with aliquots of $[Pd(^{15}NH_2CH_2CH_2{}^{15}NH_2)(NO_3)_2]$ in H_2O/D_2O (9:1) appropriate for anticipated conversion to complexes **4**−**6**. The solutions were adjusted to pH 4.2−4.4, using 0.01 M NaOH and 0.01 M HNO_3, and ^{1}H NMR spectra revealed formation of a single species in each case.

^{15}N NMR spectra (Figure 7) were also recorded for these solutions and verify the formation of a single species (**4**, **5**, or **6**) from each reaction. Figure 7c showed six resonances for **6** (δ_N −16.3 (two overlapped signals), −16.8, −16.9, −17.1, −17.4 ppm) corresponding to three $Pd(en)^{2+}$ moieties bound to six His* imidazole N1 nitrogen atoms from a single peptide **3**. Figure 7a,b, respectively, show four signals for **4** (δ_N −16.2, −16.2, −16.5, −16.7 ppm) and **5** (δ_N −16.3, −16.3, −16.6, −16.7 ppm) in which two $Pd(en)^{2+}$ moieties are each bound to two His* residues through imidazole N1. The locations of these resonances are consistent with inequivalent (peptide) nitrogen donor ligands trans to nitrogens for each of two (for **4**, **5**) or three (for **6**) ethylenediamine ligands. None of the amide nitrogens of peptides **1**−**3** can be coordinated to Pd(II) because they all bear a proton in the ^{1}H NMR spectra.

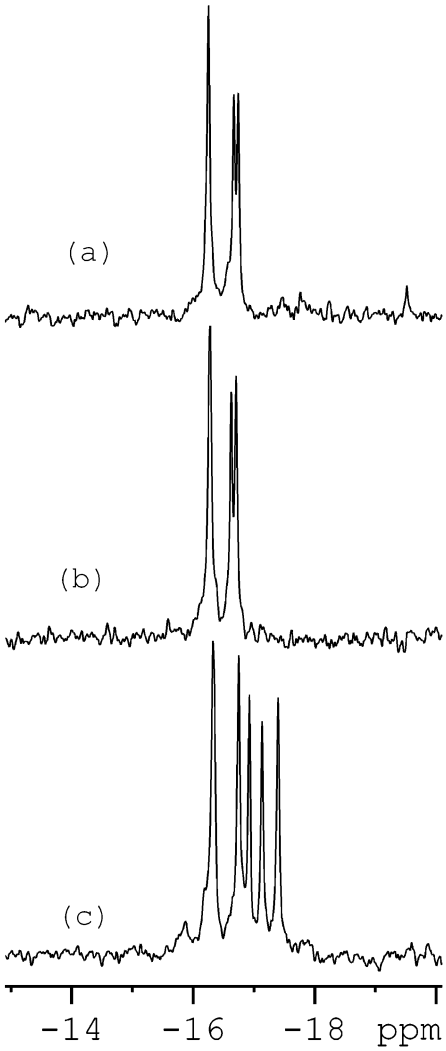

Figure 7. ^{15}N NMR spectra (40.5 MHz) for reactions in H_2O/D_2O (9:1, pH 4.2) between $[Pd(^{15}NH_2CH_2CH_2{}^{15}NH_2)(ONO_2)_2]$ and peptides (a) **1** (+2 equiv Pd), (b) **2** (+2 equiv Pd), and (c) **3** (+3 equiv Pd), showing respective formation of **4** (δ_N −16.22, −16.22, −16.52, −16.66 ppm), **5** (δ_N −16.28, −16.28, −16.63, −16.71 ppm), and **6** (δ_N −16.33, −16.33, −16.75, −16.92, −17.34, −17.40 ppm).

Unlike DMF solutions, circular dichroism spectra (Figure 8) could be measured for the peptides in water to corroborate our assertion of higher structure for **6** than for **4**, although there was some absorption by the metal moiety. Peptides longer than 15 residues that are α-helical typically give prominent double minima (222, 208 nm) and a large positive molar ellipticity at 190 nm. The relative percent helicity can theoretically be quantitated for long peptides by the mean residue ellipticity (MRE) at 222 nm.[42] Although shorter peptides do not usually

(40) Brünger, A. T. *X-PLOR Manual*, version 3.1; Yale University: New Haven, CT, 1992.
(41) Wienken, M.; Zangrando, E.; Randaccio, L.; Menzer, S.; Lippert, B. *J. Chem. Soc., Dalton Trans.* **1993**, 3349.
(42) (a) Chen, Y.-H.; Yang, J. T.; Chau, K. H. *Biochemistry* **1974**, *13*, 3350−3359. (b) Lyu, P. C.; Sherman, J. C.; Chen, A.; Kallenbach, N. R. *Proc. Natl. Acad. Sci. U.S.A.* **1991**, 88, 5317.

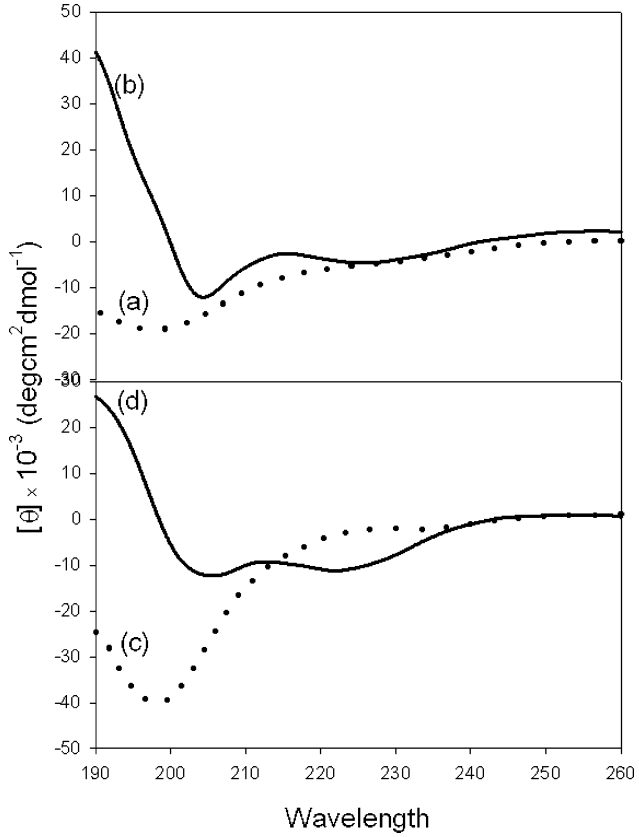

Figure 8. CD spectra for peptides **1** and **3** ± [Pd(en)$(ONO_2)_2$] in aqueous phosphate buffer at pH 6.9. (a) 10-mer **1**, (b) **1** + 2 equiv Pd (i.e., **4**), (c) 15-mer **3**, (d) **3** + 3 equiv Pd (i.e., **6**). CD spectra are similar at pH 4.2.

conform well to this relationship, we considered it worthwhile to calculate helicity at 222 nm for free and metal-bound peptides to give a rough guide as to their rank order of helicity. Using the mean residue elipticity (MRE) at 222 nm and recognizing that this method of quantifying helicity probably gives an underestimate for short peptides, we calculated[42] peptide helicity as **1**−**3** (<5%), **4** (21%), and **6** (41%).

Thus, the free peptides have negligible structure (<5% helicity) in water, consistent also with their minima ∼195−200 nm, which is typical of random structures in water. The 10-residue peptide **4** and 15-residue peptide **6**, possessing "back to back" metal clips, exhibited spectra expected for helical peptides. The MRE ratio $[\theta]_{222}/[\theta]_{208}$ is sometimes a useful indicator of the nature of the helix, being ∼0.7−1 for α-helicity but lower (∼0.4−0.7) for 3_{10}-helicity.[43] We find $[\theta]_{222}/[\theta]_{208}$ ∼0.99 for **6** and ∼0.53 for **4**, suggesting possibly a greater proportion of 3_{10}-helix in the conformational mix for **4** compared with a higher α-helix content for **6**.

Figure 9 summarizes coupling constants $^3J_{NHC\alpha}$ (≤6 Hz), amide NH temperature coefficients $\Delta\delta/T$ (≤4 ppb/K), and NOE correlations (sequential and medium range) for the in situ reaction products **4**−**6** in H_2O/D_2O (9:1). For all three compounds there are fewer low coupling constants and small temperature coefficients (Table S2, Supporting Information) than observed in DMF (Figure 5), and in particular, there are fewer $i \rightarrow i + 3$ and $i \rightarrow i + 4$ NOE correlations. Also, the CH_α chemical shift differences between **1**−**3** and **4**−**6** (Supporting

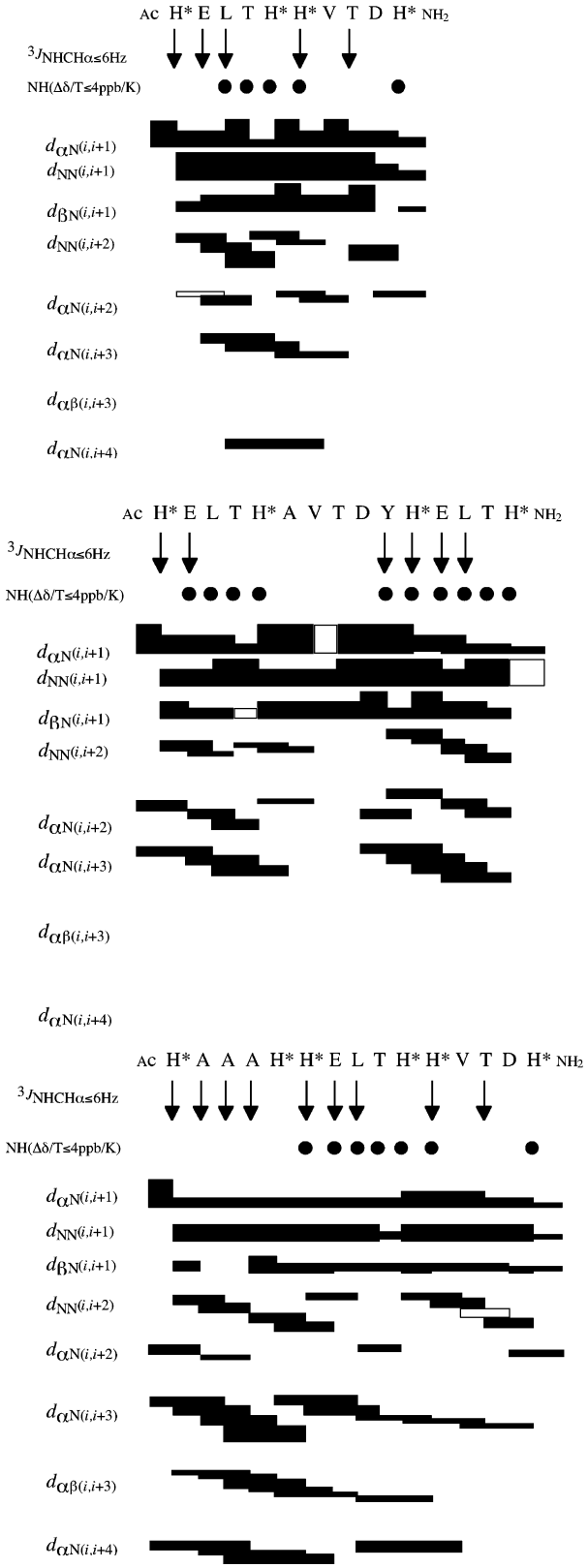

Figure 9. Summary of coupling constants $^3J_{NHC\alpha}$ (≤6 Hz shown by ↿), amide NH temperature coefficients $\Delta\delta/T$ (≤4 ppb/K shown by ●), and NOE correlations (sequential and medium range, gray bars indicate spectral overlap) for metallopeptides **4** (top), **5** (middle), **6** (bottom) in H_2O/D_2O (9:1).

Information) are consistent ($\Delta\delta$ < 0 to −0.1 ppm) with more helical structure in **6** > **4** > **5**, and this seems to suggest that the intervening residues in **5** between the metal clips (AVTDY)

(43) Zhou, N. E.; Kay, C. M.; Hodges, R. S. *Biochemistry* **1992**, *31*, 5739−5746. (b) Garcia-Echeverria, C. *J. Am. Chem. Soc.* **1994**, *116*, 6031−6032.

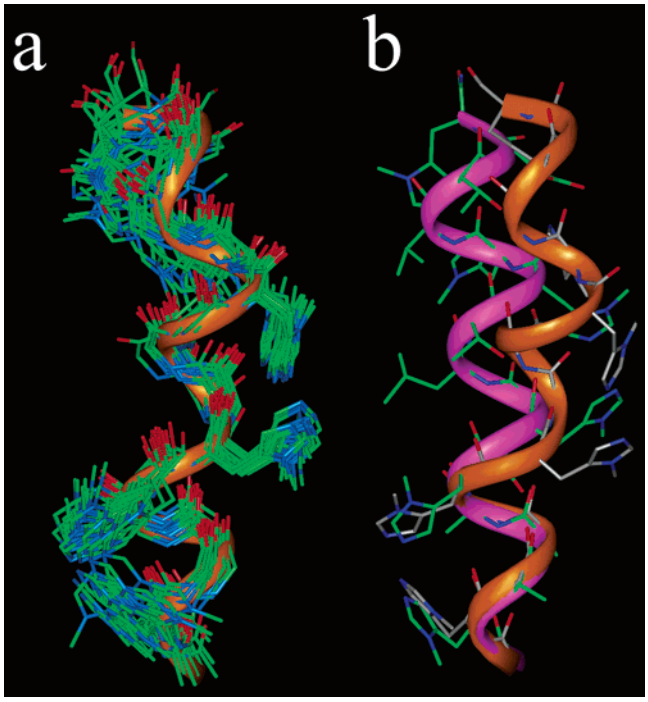

Figure 10. Backbone superimposition of (a) 20 lowest energy calculated structures for **6** in 9:1 H_2O/D_2O (av backbone pairwise rmsd 1.16 Å). Only side chains of Pd-bound His* residues are displayed along with lowest energy conformer (orange) and (b) lowest energy conformers for **6** in DMF (pink) and H_2O (orange) (backbone rmsd 1.43 Å). N-Termini at base of figure.

are not highly helix-favoring in water. We concluded from all these data that there is much less structure for **4**−**6** in water than in DMF, with possibly sufficient structure in **6** alone in water to permit a structure calculation.

Chemical shifts for amide NH resonances in complex **6** were most dispersed at 303 K (Table S8, Supporting Information); thus, 2D NMR data at this temperature (Figure 9) were used for easier characterization. The helical nature of compound **6** was supported by (a) upfield shifts of the CH_α signals relative to the free peptide **3** (Figure S11c, Supporting Information), (b) nine coupling constants where $^3J_{NHCH\alpha} \leq 6$ Hz,(c) seven amide−NH chemical shifts with low temperature dependence ($\Delta\delta/T \leq 4$ ppb/K^{-1}), consistent with the presence of hydrogen bonds, and (d) some characteristic nonsequential cross-peaks in the NOESY spectra ($d_{\alpha N(i,i+3)}$, $d_{\alpha N(i,i+4)}$, $d_{\alpha\beta(i,i+3)}$). A structure was calculated for compound **6** in H_2O/D_2O (9:1) using 251 NOE distance restraints (119 intraresidue, 68 sequential, 64 medium range) and 9 backbone ϕ angles derived from $^3J_{NHCH\alpha}$ values (Table S8, Supporting Information), using a dynamic simulated-annealing and energy-minimization protocol in X-PLOR without explicit hydrogen bond or $[Pd(en)^{2+}]$ restraints to minimize structure biasing. The N1 atoms of the His* residues spaced i and $i + 4$ residues apart were constrained to 2.7 Å as above.

The calculated lowest energy solution structures for **6** in water are displayed in Figure 10a and compared with the lowest energy average structure of **6** in DMF (Figure 10b). The calculated structure is α-helical, consistent with the characteristic NMR paramaters and CD spectra described above, with four helical turns in evidence. However, the family of lowest energy structures is less superimposable for water (Figure 10a) than for DMF (Figure 5c), and in comparing the lowest energy structure in each family (Figure 10b), the water structure is clearly skewed relative to the DMF structure due to elongation and kinking. The NOE summary diagrams (Figures 5 and 9) show a smaller ratio of $(i \rightarrow i + 4)/(i \rightarrow i + 2)$ NOEs in the protic solvent water than in the aprotic solvent DMF, consistent with less peptide structure because of greater competition from water for the backbone amide carbonyls. In other words, there are fewer intramolecular helix-defining H-bonds and less α-character in water than DMF, reflecting greater contributions to the overall structure by more heavily populated alternate conformations such as the 3_{10}-helix. This agrees with the CD spectral results above.

Solution Structures by NAMFIS Analysis. A second approach to determination of structure in solution is NAMFIS. Unlike the simulated annealing method which focuses all NMR variables (NOE distances and ^3J-related dihedral angles) on calculating the averaged lowest energy structures, NAMFIS parses the same variables among the members of a collection of conformations in rapid equilibrium.[27,28] The method deconvolutes an averaged NMR spectrum into contributing components, identifies individual conformational minima, and assigns weights to the participating conformers. Thus, the burden of accommodating the complete set of averaged data is shared among 5−20 unstrained, low-energy conformers. This assumes, of course, that a mixture of conformers, and not a single structure, properly describes the problem in question. However, were a single unique conformation the only one present in solution, NAMFIS would assign a particularly high weight to it. For compound **6**, we are dealing with three concatenated 22-membered ring cyclic pentapeptides, each of which is characterized by considerable conformational mobility (see below). It is expected that 10−15-mers such as **4**−**6** exist as a small collection of mobile forms despite the three locally rigid Pd clips. Accordingly, we have examined the solution structure of the metalated peptide **6** with NAMFIS, an approach belonging to a family of methods designed to address the multiple-conformation problem.[44]

NAMFIS Analysis of Pentapeptides Pd^{2+}[H*AAAH*] (7), Pd^{2+}[H*ELTH*] (8), and Pd^{2+}[H*VTDH*] (9). The conformational hypersurface of tripalladated peptide **6** is exceptionally complex. Each of the 22-membered rings contains 14 easily rotated ring bonds. Four additional single bonds link the cyclic units, while eight extended side chains contribute numerous torsions to the mix. There are essentially two extreme assumptions that can be made about the level of conformational complexity for such molecules. The first is that the 15-mer **6** adopts a single backbone conformation in solution, and the second is that **6** explores all possible conformational families as a rapidly equilibrating mixture. The present NAMFIS analysis attempts to address whether the original design motif focusing on α-helical properties limits the conformational space to just a few structures in equilibrium.

Given that there are a total of 46 backbone bonds in **6** that define its overall secondary structure, we are unable to explore

(44) (a) Landis, C.; Allured, V. S. *J. Am. Chem. Soc.* **1991**, *113*, 9493−9499. (b) Landis, C. R.; Luck, L. L.; Wright, J. M. *J. Magn. Reson., Ser B* **1995**, *109*, 44−59. (c) Wright, J. M.; Landis, C. R.; Ros M. A. M. P.; Horton, A. D. *Organometallics* **1998**, *17*, 5031−5040. (d) Nikiforovich, G. V.; Vesterman, B. G.; Betins, J. *Biophys. Chem.* **1988**, *31*, 101−106. (e) Mierke, D. F.; Kurz, M.; Kessler, H. *J. Am. Chem. Soc.* **1994**, *116*, 1042−1049. (f) Cuniasse, P.; Raynal, I.; Yiotakis, A. *J. Am. Chem. Soc.* **1997**, *119*, 5239−5248.

Table 2. NAMFIS Analysis of Pentapeptide Fragments **7**−**9** from the NMR Spectrum of Metalated Peptide **6** in DMF-d_7

peptide (SSD)		conformation	% pop in solution	structural classification
7 (176)	1	Ace-CO- - -HN-A4; 1H*-CO- - -HN−H*5	45	constrained α-helix
	2	Ace-CO- - -HNter	20	loop
	3	1H*-NH- - -OC−H*5; 1H*-CO- - -HN-A3; A3-CO- - -HNter	7	mixed
	4	A2-CO- - -HN-A4; A3-CO- - -HN−H*5	5	double γ-turn
	5	A2-NH- - -OC−H*5; A2-CO- - -HN−H*5	5	β-turn
	6	Ace-CO- - -HN-A3; H*1-CO- - -HN−H*5	4	mixed
	7	H*1-NH- - -OC−H*5; H*1-CO- - -HN−H*5	4	α-helix
	8	no backbone H-bonds	3	loop
	9	A2-HN- - -OC−H*5; A2-CO- - -HN−H*5	3	β-turn
8 (369)	1	H*1-CO- - -Hnter; L3-NH- - -OC−H*5	42	γ-turn
	2	Ace-CO- - -HN-L3; H*1-CO- - -HN-T5; L3-CO- - -HN−H*6	25	3,10 helix
	3	H*1-NH- - -OC−H*6; H*1-CO- - -HNter	10	loop
	4	no backbone H-bonds	7	loop
	5	2E-CO- - -HN-5T	7	γ-turn
	6	3L-NH- - -OC−H*6	5	loop
	7	no backbone H-bonds	4	loop
9 (270)	1	no backbone H-bonds	45	loop
	2	Ace-CO- - -HNter	25	loop
	3	no backbone H-bonds	17	loop
	4	no backbone H-bonds	4	loop
	5	no backbone H-bonds	4	loop

Table 3. NAMFIS Analysis of Pentapeptide Fragments **7**−**9** from the NMR Spectrum of Metalated Peptide **6** in D_2O

peptide (SSD)		conformation	% pop in solution	structural classification
7 (234)	1	A2-NH- - -OC−H*5; A2-CO- - -HN−H*5	59	β-turn
	2	Ace-CO- - -HN-A3	14	3,10 helix
	3	1H*-NH- - -OC−H*5	7	α-helix
	4	Ace-CO- - -HN-L3; H*1-CO- - -HN-T5; L3-CO- - -HN−H*6	5	3,10 helix
	5	no backbone H-bonds	5	loop
	6	H*1-NH- - -OC−H*5; H*1-CO- - -HN-A3	4	mixed
	7	Ace-CO- - -HN-A4	2	α-helix
8 (320)	1	Ace-CO- - -HN-T4; H1−CO- - -HN−H*5; E2-CO- - -HNter	96	α-helix
	2	T4-CO- - -HNter	4	loop
9 (403)	1	no backbone H-bonds	77	loop
	2	V2−CO- - -HN-D4	5	γ-turn
	3	no backbone H-bonds	3	loop
	4	H*1-CO- - -HN-T3	2	γ-turn
	5	no backbone H-bonds	2	loop
	6	H*1-CO- - -HN-T3; H*1-NH- - -OC-D4	2	mixed
	7	V2−CO- - -HN-D4	2	γ-turn

the reaches of conformational space. Consequently, each of the constituent metalated pentapeptides of **6** (Pd^{2+}[H*AAAH*] (**7**), Pd^{2+}[H*ELTH*] (**8**), and Pd^{2+}[H*VTDH*]) (**9**) was separately subjected to an extensive conformational search and subsequently analyzed by NAMFIS using the NOEs and $^3J_{NHCH\alpha}$'s recorded for that section of **6** (Tables 2 and 3). Precedence for such a technique is found in the NMR-based conformational analysis of a 13-residue peptide with an 8-residue loop reported simultaneously with the initial presentation of the NAMFIS approach.[27] Thus, the three Pd^{2+} cyclic peptides were each subjected to a 180 000-step Monte Carlo conformational search with AMBER*/GBSA/H2O and a 7 kcal/mol energy window in MacroModel 6.5 to obtain conformational datasets of 1835, 1345, and 1270 conformers for **7**−**9**, respectively. As noted in the Experimental Section, each set was supplemented with two helical conformations: the idealized α-helical conformer and the corresponding 3_{10}-helix derived by unconstrained optimization of the α-helix form. Results from conformer deconvolution in DMF-d_6 and D_2O are presented below.

NAMFIS Analysis of $[Pd_3(en)_3$(Ac-H*AAAH*H*-ELTH*H*VTDH*-$NH_2)]^{4+}$ (6) in DMF-d_7. The 62 local NOEs and 5 $^3J_{NHCH\alpha}$'s of pentapeptide **7** (Pd^{2+}[H*AAAH*]) were NAMFIS-adapted to 1837 AMBER*-optimized conformers. The "best fit" of the data provides an ensemble of nine conformations with populations ranging from 45 to 3% (Table 2). The most populated conformer is the ideal α-helix. The remaining structures are characterized by loops and γ-turns, with the 3_{10}-helical form not appearing among them. The corresponding analysis for the 1347 conformers of Pd^{2+}[H*ELTH*] (**8**) provides seven conformers, the most populated of which is a γ-turn (42%). The 3_{10}-helix is the second most populated conformation (25%), while the remaining solution forms are posited to incorporate loops (total population of 26%) and a γ-turn (7%). Finally, the 1272 conformers of Pd^{2+}[H*VTDH*] deliver five NAMFIS selections with populations in solution ranging from 45 to 4%. All are distinguished by loops with no defined secondary structure.

For analysis of tri-Pd peptide **6** in DMF-d_6, all NMR parameters (279 NOEs and 15 $^3J_{NHCH\alpha}$'s) were used by NAMFIS, with the set of conformers limited to six structures: the ideal α-helix, $\mathbf{H_{DMF}}$, the α- and (3,10)-mixed helices $\mathbf{H'_{DMF}}$, $\mathbf{H''_{DMF}}$, and $\mathbf{H'''_{DMF}}$ (Figure 11), and ideal NAMFIS conformers $\mathbf{N_{DMF}}$ and $\mathbf{N'_{DMF}}$ (Figure 12a,b). NAMFIS matching of the NMR-determined variables against the set of six conformations delivers one main contributor to the solution ensemble: $\mathbf{H''_{DMF}}$ (92%). The remaining 8% is composed of $\mathbf{H'''_{DMF}}$, $\mathbf{N_{DMF}}$, and $\mathbf{N'_{DMF}}$. Thus, the major form predicted for **6** in DMF-d_6 is the optimized ideal α-helix with backbone *i*, *i* + 4 hydrogen bonds extending the length of the helix, except for peptide fragment **9**, which presents as a 3_{10}-helix. Accordingly, the predominant structure obtained from NAMFIS treatment of the DMF data (Figure 11, $\mathbf{H_{DMF}}$) is in very close agreement with the simulated annealing derived structure for **6** depicted in Figures 6c and 10.

NAMFIS Analysis of 6 in D_2O. Treatment of the pentapeptide components **7**−**9** using the heavy water data for trimetalated **6** was identical to that utilized for the DMF-d_7 data (Table 3). Pd^{2+}[H*AAAH*] (**7**) yielded seven conformations in water, with populations ranging from 59 to 2%, two less than in DMF, although the fit is slightly poorer. Significantly, the most populated conformer is a β-turn exhibiting two hydrogen bonds between A2-NH···OC−H*5 and A2-CO···HN−H*5, while the second largest structural class is the 3_{10}-helix comprising 21% of the population. Unlike the results in DMF, the α-helical forms that may be present in solution for **7** are estimated to amount to only 9% of the population.

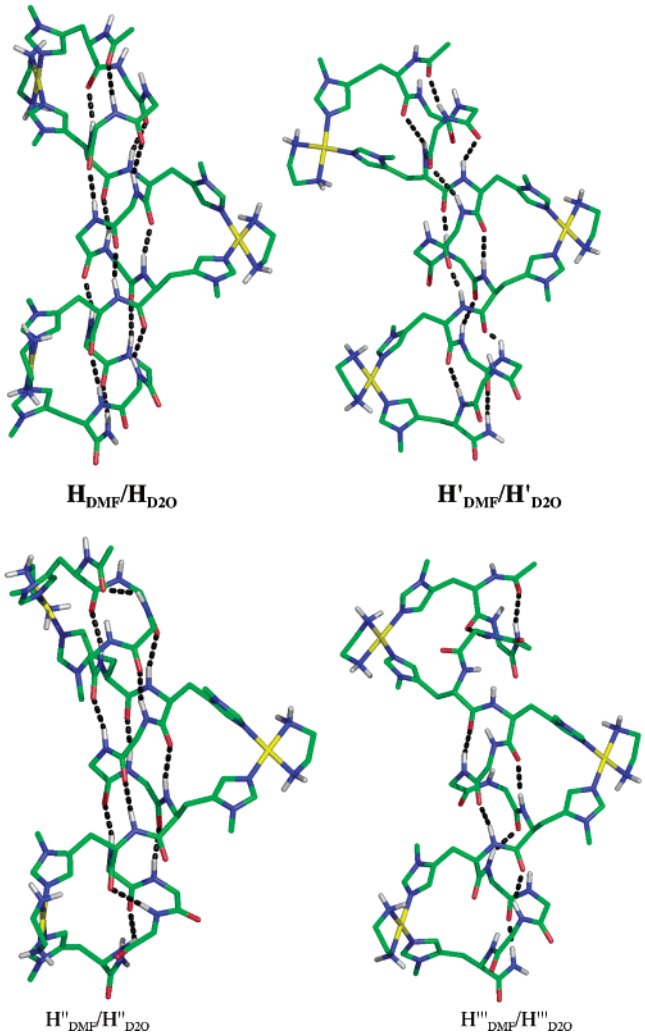

Figure 11. Representative helical structures of **6** employed in NAMFIS deconvolution. $\mathbf{H_{DMF}/H_{D2O}}$ is a constrained ideal α-helix, $\mathbf{H'_{DMF}/H'_{D2O}}$ constitutes constrained ideal α-helical fragments for **7**−**9** with (3,10) connectors, and $\mathbf{H''_{DMF}/H''_{D2O}}$ and $\mathbf{H'''_{DMF}/H'''_{D2O}}$ are unconstrained optimized forms of $\mathbf{H_{DMF}/H_{D2O}}$ and $\mathbf{H'_{DMF}/H'_{D2O}}$, repectively.

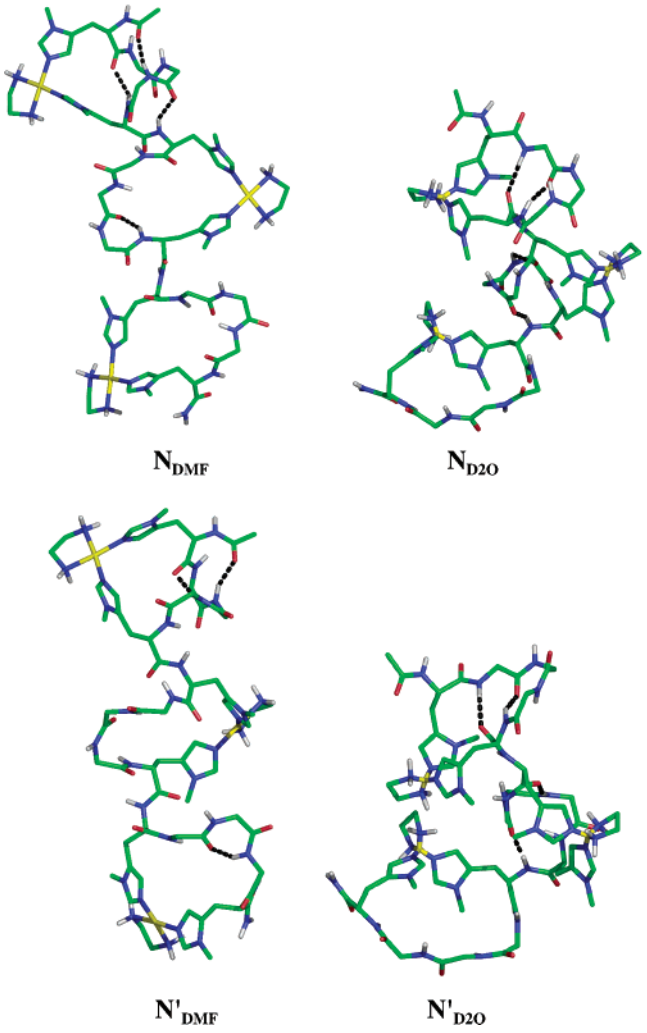

Figure 12. Representative structures of the top conformers derived from the individual NAMFIS analysis on **7**−**9** in DMF and D_2O ($\mathbf{N_{DMF}}$; $\mathbf{N_{D2O}}$) and unconstrained minimization of $\mathbf{N_{DMF}}$ and $\mathbf{N_{D2O}}$ ($\mathbf{N'_{DMF}}$; $\mathbf{N'_{D2O}}$, respectively).

Pentapeptide **8**, Pd^{2+}[H*ELTH*], delivers only two conformations from the 1347 conformer dataset. Remarkably, the ideal α-helix makes up 96% of the population. Fragment **9**, Pd^{2+}-[H*VTDH*], results in a seven-conformer "best fit", with populations in solution ranging from 77 to 2%. The most populated form (77%) is a loop structure with a single hydrogen bond from the threonine side chain (D4-NH···OH-T3). The remaining structures are characterized by loops, with the exception of the 9% population composed of γ-turns.

Tripeptide **6** shows 251 NOEs and 11 $^3J_{NHC\alpha}$'s in D_2O. The "best fit" of the data against the six conformers noted above results in the contribution of two main forms: $\mathbf{H'_{D2O}}$ (73%) and $\mathbf{N'_{D2O}}$ (27%). The idealized α-helix contributes a diminutive 0.5% to the equilibrium population. Nonetheless, the lead conformer is composed of 70/30 α-helix/3_{10}-helix, while the second equilibrium partner sustains 20−30% α-helical character. The combination is semiquantitatively consistent with the CD estimate for **6** that 41% is a lower boundary for peptide helicity. It furthermore supports the conclusion above that there is more helicity in DMF than in D_2O.

That the NAMFIS analysis for tripalladated peptide **6** is in agreement with the simulated annealing approach is satisfying in that both methods predict a high degree of helicity for the molecule in both DMF and D_2O. However, the result from both methods should be considered to be more qualitative than quantitative. A measure of the accuracy of the fit between NMR-derived geometry parameters and conformation is given by the SSD statistic.[27,28] Generally, this value falls below 200, and occasionally below 100.[18,27,28,45] Tables 2 and 3, summarizing the NAMFIS results for pentapeptides **7**−**9,** record SSD values from 176 to 403, slightly outside the range normally observed. More significant, however, is that the SSDs from the analysis of 15-mer **6** in DMF and D_2O are 1679 and 1570, respectively. In the present work, there are two main sources reflecting the less-than-optimal fit of the force field structures and the NMR geometrics. The first concerns the rather large number of weak NOEs employed in the analysis. The corresponding explicit but long distances required as input to NAMFIS carry a considerable degree of uncertainty. Second, because of the expansiveness of the actual conformational surface for **6**, we have employed only a limited number of conformations, albeit a number of ideal

(45) (a) Monteagudo, E.; Cicero, D. O.; Cornett, B.; Myles, D. C.; Snyder, J. P. *J. Am. Chem. Soc.* **2001**, *123*, 6929−6930 (SI). (b) Baroni, L.; Lambertucci, C.; Appendino, G.; Vander Velde, D. G.; Himes, R. H.; Bombardelli, E.; Wang, M.; Snyder, J. P. *J. Med. Chem.* **2001**, *44*, 1576−1587.

and near-ideal helical structures. The large SSDs for the molecule suggest that the weights recorded above represent an upper limit on the presence of the helical conformations. Were we able to have used a more representative and diversified set of conformations for **6**, the SSDs and the populations of the helical entities would likely diminish. Nevertheless, we believe the relative degree of helicity from DMF to D_2O to be reliable and supportive of both the NMR and CD interpretations.

Conclusions

The electrophilic $Pd(en)^{2+}$ has been found to be a remarkably regioselective peptide-binding probe or "metal clip" that is also helix-inducing. Coordination to three 10−15 residue peptides possessing a number of potential metal-binding donors, including 4−6 histidines in a variety of positions, was highly regioselective, with the thermodynamically stable products bearing 22-membered metal chelate rings each involving (i, $i + 4$) histidines coordinated via imidazole N1 to Pd(II). This stable macrocycle $[Pden(HxxxH)]^{2+}$ is closely analogous to metal-bound regions in metalloproteins, but quite unlike reported short peptide binding modes in small inorganic complexes, where five- and six-membered rings predominate. We attribute the regioselective (i, $i + 4$) coordination and the resultant stability of the 22-membered ring to unique presentation of i, $i + 4$ His residues on the same peptide face, as occurs in a helical turn, the proximity enabling chelation to cis-positions on the $Pd(en)^{2+}$ moiety.

This unusually large metallocycle also lowers the entropic barrier to folding into an α-helical turn by organizing component H-bond donors and acceptors into positions mimicking the pitch and spacing of carbonyl oxygens and amide NHs in native protein α-helices. We used this stable macrocycle here as an α-turn-mimicking module to build short, otherwise unstable, peptide helices. Multiple ($n = 2, 3$) units of $([Pd(en)(H*XXXH*)]^{2+})_n$ could be formed in situ in one step within 10−15 residue peptides. This modular strategy induced non-helical peptides to become highly α-helical metallopeptide sequences. We deliberately chose to use free peptides that displayed no helicity at all in solution, as verified by CD spectra in water and NOESY spectra in DMF and water. This contrasts with the few other reports in this field, where metal ions induced helicity in already fairly helical peptides.

The observations of much greater helical structure in the aprotic dipolar solvent DMF than in the protic solvent water may be very relevant for proteins, where this and other HxxxH sequences tend to be buried in quite hydrophobic environments rather than located on water-exposed protein surfaces. Our use of the N3-methyl histidines here, to simplify NMR analysis, does not detract from the fact that the species we see are also accessible by unsubstituted His residues as previously reported.[17a] The HxxxH signature is extremely common both in metalloproteins and in proteins not previously associated with metal ions. This work supports the possibility that metal ions could have important templating roles during protein folding. It is conceivable that even transient coordination of labile (first row transition) metal ions could template helix-folding. Once helices become sufficiently long, or when helix-stabilizing hydrophobic protein environments become created through folding, the metal template may no longer be required to preserve the thermodynamic stability of a helix and could be displaced from some proteins by other metal-binding ligands. Roles for metal-induced helix formation in peptides and proteins should certainly be investigated further.

Acknowledgment. D.P.F. and T.G.A. thank the Australian Research Council for financial support for this research and for an Australian Professorial Fellowship (D.P.F.). Drs. Martin Stoermer, Matthew Glenn, and Bernhard Pfeiffer are acknowledged for assistance in acquiring some NMR spectra and Alun Jones is thanked for help in acquiring mass spectra (Queensland). J.P.S. and A.S.L. are grateful to Professor Dennis Liotta (Emory University) for encouragement and support.

Supporting Information Available: Figures S1−S10 and Tables S1−S7 provide extensive additional multinuclear and multidimensional NMR data for peptides **1**−**6** (PDF). This material is available free of charge via the Internet at http://pubs.acs.org.

JA037980I